New paleointensity results from rapidly cooled Icelandic lavas: Implications for Arctic geomagnetic field strength

G. Cromwell,[1,2] L. Tauxe,[1] and S.A. Halldórsson[1,3]

G. Cromwell, Occidental College, 1600 Campus Rd, Los Angeles, CA 90041, USA

L. Tauxe, Geosciences Research Division, Scripps Institution of Oceanography, University of California San Diego, 9500 Gilman Dr, La Jolla, CA 92093-0220, USA

S.A. Halldórsson, Nordic Volcanological Centre, Institute of Earth Sciences, University of Iceland, Askja, Sturlugata 7, 101 Reykjavík, Iceland

[1]Geosciences Research Division, Scripps Institution of Oceanography, University of California San Diego, La Jolla, California, USA

[2]Now at: Occidental College, Los Angeles, California, USA

[3]Now at: Nordic Volcanological Centre, Institute of Earth Sciences, University of Iceland, Reykjavík, Iceland

Abstract. The Earth's magnetic field is assumed to be a geocentric axial dipole (GAD) when averaged over over sufficient time ($10^5 - 10^6$ yrs). Recent investigations of global paleosecular variation and time averaged field behavior on million year timescales generally support a predominantly dipole field in the northern hemisphere, but unique field structures at high southern latitudes suggest the presence of a substantial $\bar{g}_2^0$ component. Average paleointensity results from Antarctica are approximately half the value predicted by a GAD field; this behavior has not been sufficiently investigated because there is a paucity of absolute paleointensity data from the Arctic and no adequate comparisons have been made between the two regions. We collected glassy volcanic material from 129 subaerial and subglacial volcanic units in Iceland in order to provide a suitable intensity data set at high northern latitudes. Forty-four sites met our very strict specimen and site level selection criteria. Four Holocene sites have a median intensity value of 55.8 ± 15.6 μT (VADM=78.1 ± 22.0 ZAm^2), consistent with the present day field. Thirty-seven sites are between 11 ka and 3.5 Ma with a median intensity of 33.1 $\pm$ 8.3 μT (47.0 $\pm$ 11.6 ZAm^2). This median intensity is indistinguishable from some long-term global field strength estimates. Reevaluation of existing high latitude data suggests a general agreement with or Iceland results, but there are still too few Antarctic sites to adequately compare Arctic and Antarctic field behaviors.

1. Introduction

The Earth's ancient magnetic field can be approximated by a geocentric axial dipole (GAD) in which the average field intensity is twice as strong at the poles as it is at the equator. The present day geomagnetic field and the Holocene time averaged field (e.g., *Korte et al.* [2011]) generally support the GAD hypothesis with a virtual axial dipole moment (VADM) of about 80 ZAm^2, but both also suggest some hemispheric asymmetry in the average field. A VADM of 80 ZAm^2 corresponds to surface field intensities of $\sim$30 μT and 60 μT at the equator and poles, respectively (red line in Figure 1).

In a departure from the long standing belief that the present field strength is representative of the long term average (e.g., *Tanaka et al.* [1995a]), *Juarez et al.* [1998] suggested that the long-term average field (5-160 Ma) was $\sim$42 ZAm^2 (supported more recently by *Tauxe et al.* [2013] for 0-140 Ma), implying equatorial and polar fields of $\sim$16 μT and $\sim$ 32 μT, respectively (blue dashed line in Figure 1). In line with this prediction, [*Lawrence et al.*, 2009] found an average field of 31.5 ± 2.4 μT in Antarctica, similar to the predictions of *Juarez et al.* [1998] and *Tauxe et al.* [2013] (compare blue dashed line with $\sim$80°S bin in Figure 1).

In contrast to the decidedly non-GAD behavior in the published intensity data shown in Figure 1, directional data, in particular, inclinations, are much more consistent with a GAD field with only small contributions from non-GAD components required to fit the data for the last few million years (e.g., *Kelly and Gubbins* [1997]; *Johnson and Constable* [1996]; *Glatzmaier et al.* [1999] and *Cromwell et al.* [2014a]). An explanation for the paleointensity departures from GAD is geodynamic differences in the outer core (e.g., *Olson and Aurnou* [1999]; *Jackson et al.* [2000]; *Hulot et al.* [2002]; *Gubbins et al.* [2006]) expressed as maximum and minimum

flux zones within the tangent cylinder (e.g., *Christensen et al.* [1998]). Some time averaged field models such as CALS10k.1b [*Korte et al.*, 2011], GUFM1 [*Jackson et al.*, 2000] and paleosecular variation (PSV) studies (e.g., *Johnson and Constable* [1996]) observe unusual field structures at high latitudes, notably the presence of persistent flux lobes in both the Arctic and Antarctic regions. A comparison of Arctic and Antarctic paleointensity results over similar timescales (0-5 Ma) might offer insights into the long term behavior of the geomagnetic field at high latitudes.

Figure 1 shows that there are many paleointensity results from high northern latitudes. The majority of these studies have been conducted in Iceland, which is located just below the Arctic circle. As a result of $\sim$15 million years [*McDougall et al.*, 1984] of continuous volcanism, Iceland contains a nearly endless number of well-exposed subaerial and subglacial volcanic sequences. Major objectives of most paleomagnetic studies in Iceland have been to provide magnetostratigraphic controls for local geologic formations (e.g., *Walker* [1959]; *Watkins and Walker* [1977]; *McDougall et al.* [1984]; *Kristjánsson et al.* [1998]; *Helgason and Duncan* [2001]; *Kristjánsson* [2010]), evaluate secular variation of the ancient geomagnetic field (e.g., *Tanaka et al.* [1995b]; *Udagawa et al.* [1999]; *Kristjánsson* [2013]), and define the characteristics of geomagnetic reversals (e.g., *Shaw* [1975]; *Kristjánsson et al.* [1980]; *Goguitchaichvili et al.* [1999]) or excursions (e.g., *Marshall et al.* [1988]; *Levi et al.* [1990]; *Camps et al.* [2011]; *Jicha et al.* [2011]). Paleointensity studies in Iceland have focused primarily on transitional field events (e.g., *Lawley* [1970]; *Shaw* [1975]; *Marshall et al.* [1988]; *Goguitchaichvili et al.* [1999]; *Brown et al.* [2006]; *Ferk and Leonhardt* [2009]), while relatively little work has been done to explore the strength of the magnetic field during stable polarity intervals, which is necessary for investigations of long term geomagnetic field behavior.

Several Icelandic studies do provide intensity results that are potentially useful for Arctic/Antarctic comparisons (e.g., *Schweitzer and Soffel* [1980]; *Senanayake et al.* [1982]; *Roberts and Shaw* [1984]; *Tanaka et al.* [1995a]; *Stanton et al.* [2011] and *Tanaka et al.* [2012]). However, such investigations are dependent on the ability of lava flows to accurately record magnetic field strength. *Love and Constable* [2003], *Herrero-Bervera and Valet* [2009] and *Cromwell et al.* [2014b] compiled results from the 1960 Kilauea lava flow on the Big Island of Hawaii and found that the majority of published paleointensity estimates of the flow do not consistently recover the expected field strength. *Love and Constable* [2003] estimated that available data from the 1960 flow had a 19% standard deviation of the mean and an average field strength of 33.91 μT (expected field=36.0 μT). Different experimental techniques and selection criteria contribute to the variance in the Kilauea data, and *Cromwell et al.* [2014b] suggested that a major cause of erroneous field estimates is the type of volcanic material used in laboratory experiments.

Most paleointensity studies collect samples from the slowly cooled, massive interiors of lava flows. These samples have relatively large crystals and often produce large ($>\sim 200$ nm), multi-domain magnetic grains. It is common for multi-domain specimens to yield curved, concave-up Arai plots [*Dunlop and Özdemir*, 2001] during paleointensity experiments, frequently resulting in subjective NRM/TRM slope interpretations. Multi-domain paleointensity results are also shown to consistently underestimate expected magnetic field strength when calculating the full thermal remanent magnetization (TRM) [*Cromwell et al.*, 2013, 2014b]. Single-domain magnetic grains on the other hand, are significantly smaller ($<\sim 80$nm) and are expected to respond well to paleomagnetic experiments. Distributions of single domain particles can be found in most volcanic rock types but they comprise an especially large percentage of volcanic glasses and other quenched materials. Volcanic glass has been used for paleointensity investigations

of the ancient magnetic field (e.g., [*Pick and Tauxe*, 1993; *Tauxe and Staudigel*, 2004; *Tauxe*, 2006; *Bowles et al.*, 2006; *Ferk and Leonhardt*, 2009; *Ferk et al.*, 2011], and recently, *Cromwell et al.* [2014b] showed that rapidly cooled material from subaerially erupted Hawaiian lavas can consistently recover the expected field strength. The success of glassy material in paleointensity experiments makes it ideal for global investigations of the ancient geomagnetic field. Iceland is an excellent study location for this purpose due to the accessibility of subglacial volcanic sequences emplaced during the last $\sim$3 Ma [*McDougall et al.*, 1977; *Helgason and Duncan*, 2001] and possibly as far back as late Miocene time [*Geirsdóttir and Eiríksson*, 1994].

In this study we present a new collection of Icelandic volcanic glasses from subglacial and subaerial lava flows in order to evaluate the paleointensity in Iceland over the last few million years. We apply strict selection criteria to ensure an accurate representation of field strength and then compare our results to current field models and published high latitude data that pass our selection criteria. Here we discuss the time averaged strength of the geomagnetic field in the Arctic and the possibility of long-term hemispheric asymmetry at high latitudes.

2. Geologic Setting

Iceland is a volcanic island situated on the Mid-Atlantic Ridge at the boundary between the North American and Eurasian plates (Figure 2). Iceland has an unusually thick crust due to a high degree of melting associated with a mantle hotspot beneath the island [*Bjarnason and Schmeling*, 2009]. Constant spreading between the North American and Eurasian plates means that the oldest rocks in Iceland, $\sim$15 Ma, are found in the eastern and westernmost parts of the island, with progressively younger formations generally occurring closer to the spreading axis. Active volcanism occurs in the neovolcanic zone (0-0.78 Ma) which transects the length of the island from the Reykjanes Pensinsula in the southwest to the Tjörnes-Axarfjördur region

in the northeast (Figure 2). The neovolcanic zone is differentiated between an axial rift zone and off-rift volcanic zones. The axial rift zone spans the length of Iceland, and is divided into Western (WRZ), Eastern (ERZ) and Northern (NRZ) rift zone segments (Figure 2). Two off-rift volcanic zones are the South Iceland Volcanic Zone (SIVZ), an extension of the ERZ, and the Snaefellsnes Volcanic Zone (SNVZ), which is an intraplate volcanic system and not directly related to active plate boundary volcanism [*Einarsson*, 2008].

3. Sample Collection

Glassy volcanic samples were collected over several field seasons (pre-2006, 2008 and 2012) for isotope geochemistry and paleomagnetic analysis. Early field expeditions were initially organized by the University of Iceland and later by Dr. David Hilton's research group at Scripps Institution of Oceanography (SIO) and the University of Iceland as part of an on-going project directed at the volatile characteristics of the Iceland mantle plume [*Macpherson et al.*, 2005; *Füri et al.*, 2010; *Barry et al.*, 2014]. Fresh glassy material from these expeditions were collected from subglacial volcanic units throughout the neovolcanic zone. The 2012 field season was organized by the paleomagnetic group at SIO with the goal of adding to the existing collection of Brunhes age (0-0.78 Ma), neovolcanic glasses and by targeting subglacial units with a greater age range (0-4 Ma) in the Núpakot, Sida and Skaftafell areas (Figure 2). The 2012 sampling plan was guided by previous work on subglacial and subaerial volcanic sequences, including: *Kristjánsson et al.* [1980, 1988]; *Bergh and Sigvaldason* [1991]; *Helgason and Duncan* [2001]; *Füri et al.* [2010] and *Stanton et al.* [2011]. All sites are listed in Table 1 along with their correlated formation names, available age estimates and location information.

3.1. Neovolcanic Zone

The neovolcanic zone contains formations emplaced during the Brunhes chron (0-0.78 Ma). Most geologic formations in the neovolcanic zone are stratigraphically constrained using geologic maps (e.g., *Jóhannesson and Sæ mundsson* [2009]; *Saemundsson et al.* [2010]) and have relatively large age uncertainties. Absolute geochronology is rare because Icelandic basalts have low potassium content (e.g., *Jakobsson et al.* [2008]) which makes age estimates from traditional ^{40}K/^{39}Ar and ^{40}Ar/^{39}Ar methods difficult to acquire. ^{14}C radiometric dates are available (e.g., *Jónsson* [1974]; *Hjartarson* [1994]; *Sinton et al.* [2005]) but the absolute range of this method is limited to $\sim$50 ka. Relatively few ^{40}K/^{39}Ar and ^{40}Ar/^{39}Ar ages are available for lavas younger than 0.78 Ma (e.g., *Levi et al.* [1990]; *Jicha et al.* [2011]) but the majority of published ^{40}K/^{39}Ar and ^{40}Ar/^{39}Ar dates in Iceland are from units significantly older than 0.78 Ma (e.g., *Saemundsson and Noll* [1974]; *McDougall et al.* [1977, 1984]; *Helgason and Duncan* [2001]. Recent work by *Guillou et al.* [2010] suggests that an unspiked K-Ar method can successfully date Quaternary Icelandic lavas and potentially accommodate volcanic units emplaced between the reliability timescales of ^{14}C and traditional K-Ar series geochronology.

In general, neovolcanic geology is divided into a postglacial period ($<$ 11 ka, Holocene) dominated by subaerial lava flows (e.g. Figure 3c and d) and an older period of subglacial or interglacial ($11 - 780$ ka, Brunhes) pillow basalts (Figure 3a), hyaloclastite sequences (Figure 3b) or interglacial lava flows [*Jóhannesson and Sæ mundsson*, 2009]. Samples collected on the Reykjanes Peninsula have better age control than those in the ERZ and NRZ due to a greater level of detail of available geologic maps in southwest Iceland compared to other parts of the country. *Saemundsson et al.* [2010] subdivide the Reykjanes Peninsula into postglacial historic ($0 - 1.3$ ka) and prehistoric ($1.3 - 11$ ka) lavas, and subglacial Late Weichsel ($11 - 21$ ka), Early

Weichsel ($21 - 110$ ka) and Early Brunhes ($110 - 780$ ka) volcanic units. The Weichsel period encompasses the last glaciation from approximately $11 - 110$ ka, and peak glaciation at 21 ka separates the "Late" and "Early" periods.

In total, we sampled 80 distinct volcanic units from the neovolcanic zone. Sixty-one were collected before 2006 and 19 were collected during the 2012 field season. Four Weichsel lavas from the 2006-2008 collection (KLE-1, NES-2, OLF-1, SKARD-1) were resampled in 2012 to supplement the limited amount of material. All samples from these units are combined into the 2012 naming convention (isl004, isl011, isl012, isl013, respectively).

3.2. Núpakot

The Núpakot sampling area is located on the southern flank of the Eyjafjöll volcanic system in the SIVZ and is composed of interglacial lavas and subglacial hyaloclastite layers. *Jóhannesson* [1985] identified the Brunhes/Matuyama (B/M) polarity transition in a sequence of lavas near the Núpakot farm. Magnetostratigraphy by *Kristjánsson et al.* [1988] located the polarity transition approximately 50 meters above the base of this outcrop (Section A; all section and flow names referenced here are from *Kristjánsson et al.* [1988]), at the midpoint of a sequence of nine eruptive events. *Kristjánsson et al.* [1988] identified and numbered a total of 13 lava flows in the entire Núpakot sequence with Flow 1 located at the base. A single ^{40}K/^{39}Ar age determination, 0.78 ± 0.03 Ma [*McDougall et al.*, 1984], from the second eruptive unit above the base (Flow 2), confirms the geomagnetic polarity timescale age of the Núpakot section. In total, we collected four samples from the Núpakot area, isl059-isl062.

3.3. Sida

This area in southeastern Iceland includes two main lithostratigraphic groups: subaerial lava flows and sediments of Holocene age and an older group of Pleistocene or late Pliocene hyaloclastites. *Jóhannesson and Sæ mundsson* [2009] map three voluminous Holocene lava flows that transect the hyaloclastite group. Two lavas are historical, one from the 1783 C.E. Laki eruption and the second from the 934-940 C.E. Eldgjá event [*Thordarson and Hoskuldsson*, 2008]. The third lava is the Núpahraun flow, with an estimated age of $\sim$ 4 ka [*Jóhannesson*, 1983].

The older hyaloclastite sequence is nearly 700m thick and consists of 14 basaltic volcanic units interbedded with minor lavas and sedimentary diamictites [*Bergh and Sigvaldason*, 1991; *Banik et al.*, 2014]. No radiometric dating is available for this group of lavas but geologic maps (e.g., *Jóhannesson and Sæ mundsson* [2009]) identify the Sida group, and other areas of similar distance from the rift zone, as Pleistocene in age (0.78-3.3 Ma). *Sæ mundsson and Jóhannesson* [1980] collected paleodirectional information from Sida and determined a magnetostratigraphic age for the area spanning the Matuyama-Gauss polarity interval. In contrast, *Bergh and Sigvaldason* [1991] suggest that the fresh condition of the hyaloclastites indicates a relatively young age, perhaps not older than two or three glaciations or $<$0.3 Ma. Without absolute age controls, we follow the work of *Sæ mundsson and Jóhannesson* [1980] and adopt the Matuyama-Gauss polarity boundary age, 2.58 Ma (e.g., *Cande and Kent* [1995]), as an average age for the Sida group. This estimate is consistent with published geologic maps *Jóhannesson and Sæ mundsson* [2009], but without radiometric dating the precise geochronology for the region is uncertain and additional work may be required in the future.

193 We sampled all three Holocene lavas in the Sida area (isl047,isl048, isl049, isl052). Samples
194 isl048 and isl052 were collected from the 1783 C.E. flow in two separate locations. Samples
195 isl050, isl051, isl053-isl058, and isl063 were collected from the Matuyama/Gauss group.

3.4. Skaftafell

196 Skaftafell covers an area of about 300 km^2 and is located at the southern portion of the Vat-
197 najökull ice cap, approximately 50 km east of the EVZ. The Vatnajökull glacier surrounds
198 Skaftafell on all sides, except in the south where a low angle coastal plain runs to the shore-
199 line. Valley glaciers divide Skaftafell into four major sections: (from east to west) Svínafell,
200 Hafrafell, Skaftafellsheidi, and Skaftafellsfjöll. *Helgason and Duncan* [2001] compiled a 2-3
201 km thick composite section of subaerial lava flows, pillow basalts and hyaloclastite sequences
202 and used magnetostratigraphy and ^{40}K/^{39}Ar geochronology to describe the complex geologic
203 history of the area. New ^{40}Ar/^{39}Ar dates and detailed stratigraphy from Svínafell provide addi-
204 tional constraints on the volcanic history of that section [*Helgason and Duncan*, 2013]. At least
205 16 interglacial and glacial intervals are recorded in the volcanic strata over the last 5 Ma with an
206 increasing frequency and intensity of glacial events since $\sim$2.6 Ma. An exceptionally detailed
207 geologic map [*Helgason*, 2007] accompanies the investigation of *Helgason and Duncan* [2001].
208 The Skaftafell sections are carved by millions of years of glacial activity and have steep valley
209 faces that are accessible through stream channels and gullies. On average, the highest peaks for
210 each section reach elevations of around 1000 m above sea level with varying degrees of slope.
211 Thick lava flow sequences ($\sim$4.5 Ma) form the base of the Skaftafell area with alternating
212 layers of interglacial/glacial volcanics stacked above. The youngest dated units at the top of
213 each section are around 0.5 Ma. Most volcanic units are basaltic to intermediate in composition

214 although young acidic formations are found at the top of Skaftafellsheidi and Skaftafellsfjöll
215 and appear to be fed by an extensive dike system.

216 In total we sampled 32 volcanic units in Skaftafell; six from Svínafell (isl015-isl020), 16
217 from Skaftafellsfjöll (isl021-isl036), and 10 from Hafrafell (isl037-ial046). At Skaftafellsheidi
218 we walked up section SKH (see *Helgason* [2007]) but were unable to find any volcanic glass.

4. Methods

4.1. Paleointensity

219 Fresh-looking, glassy specimens were picked and separated from larger hand samples in the
220 laboratory. Specimens exhibiting any visible alteration features or superficial dirt were sub-
221 jected to ultrasonic cleaning in order to remove material that could acquire a thermal magnetic
222 signature during laboratory heatings. For the ultrasonic treatment, specimens were submerged
223 in a 10% HCl solution in beakers which were then placed in an ultrasonic water bath for 15 min-
224 utes. The water bath was chilled to prevent the specimens from heating above $30°$C and possibly
225 acquiring a partial thermal remanent magnetization (pTRM). Following ultrasonic cleaning, all
226 specimens with magnetic moments greater than 10^{-10}Am^2 were placed in labeled glass tubes
227 for the paleointensity experiment.

228 We used the IZZI version of the Thellier-Thellier paleointensity experiment [*Tauxe and*
229 *Staudigel*, 2004] which was performed at Scripps Institution of Oceanography using custom-
230 built ovens. A 2G Cryogenic Magnetometer was used to make natural remanent magnetization
231 (NRM) and pTRM measurements at each laboratory heating step. Specimens were subject to a
232 35 μT or 20 μT field during in-field steps and pTRM alteration checks were performed at every
233 other temperature increment. IZZI experiments were carried out until at least 95% of the NRM
234 was removed or when it was apparent that a specimen had altered during the heating process.

4.2. First-Order Reversal Curves

Select specimens were chosen for first-order reversal curve (FORC) analysis. FORC experiments were performed on a Princeton Measurements Vibrating Sample Magnetometer at the Institute for Rock Magnetism at the University of Minnesota. FORC data were analyzed using *FORCInel* software of *Harrison and Feinberg* [2008]. Smoothing factors for each specimen were chosen based on the optimization routine in *FORCInel* with values ranging from 4-10.

4.3. Selection Criteria

The Thellier GUI Auto Interpreter [*Shaar and Tauxe*, 2013] (part of the *PmagPy* software distribution available at http://earthref.org/PmagPy/cookbook) was used for paleointensity analysis. The Thellier GUI takes a uniform set of specimen and site level selection statistics and calculates objective interpretations of paleointensity data. Table 2 lists the selection criteria used in this study and we provide brief descriptions of each statistic (for a complete description of all paleointensity statistics see *Paterson et al.* [2014]). *SCAT* [*Shaar and Tauxe*, 2013] is a boolean statistic which uses the error on the best-fit Arai plot [*Nagata et al.*, 1963] slope to test the degree of scatter over a range of NRM/TRM data points. *FRAC* [*Shaar and Tauxe*, 2013] is calculated from the NRM fraction of a select range of NRM/TRM data points on an Arai plot and is determined using the full difference vector sum calculation. *Gap Max* [*Shaar and Tauxe*, 2013] is the maximum gap between two NRM/TRM data points determined by vector arithmetic. β (*Coe et al.* [1978]; *Tauxe and Staudigel* [2004]) measures the relative scatter around the best-fit line in an Arai plot. It is defined as the ratio of the standard error of the slope to the absolute value of the slope. *DANG* [*Tauxe and Staudigel*, 2004] is the angular difference between the NRM components used in the best-fit line and the angle that the line anchoring the center of mass makes with the origin. *MAD* [*Kirschvink*, 1980] is a measure of scatter about

the best-fit line through the NRM steps in an Arai plot. $\vec{k}'$ [*Paterson et al.*, 2014] is a measure of the degree of curvature in an Arai diagram between select temperature steps. A more curved arc has a higher value of $\vec{k}'$ and a perfectly straight line will have a $\vec{k}'$=0. A threshold value of $|0.164|$ is shown to remove a low-field bias in sites with curved Arai plots [*Paterson*, 2011; *Cromwell et al.*, 2014b].

Specimen and site level statistical requirements for this study were chosen based on the criteria of *Cromwell et al.* [2014b]. In their paleointensity analysis of modern Hawaiian lava flows, *Cromwell et al.* [2014b] determined that the expected magnetic field strength could be reproduced to within 4% after applying the criteria listed in Table 2. These are appropriately strict for paleointensity investigations on glassy volcanics because the relatively high success rate of quenched material in Thellier-type experiments allows for more stringent analysis without significantly limiting the quantity of successful sites.

5. Representative Experimental Results

In this section we examine the range of results from the IZZI paleointensity experiment and classify distributions of magnetic grain size and primary carriers for magnetic remanence. Figures 4 shows representative specimen behaviors that are most common in our Icelandic data set, including Arai plots [*Nagata et al.*, 1963] that are nearly linear (Figure 4a), slightly curved (Figure 4d) or altered (Figure 4g).

Specimens isl007b4 and isl007b3 are from the same lava flow and show some variability of within-site experimental behavior (Figures 4(a-c) and (d-f), respectively). The Arai plot for isl007b4 is very well behaved and passes all requirements while isl007b3 is slightly concave-up and fails the $\vec{k}'$ criterion. The estimated paleointensity from the curved specimen, (isl007b3, 15.8 μT), is slightly lower than its well behaved sister specimen (isl007b4, 16.9 μT) which

is consistent with observations of *Paterson* [2011] and *Cromwell et al.* [2014b]. Specimen isl009a2 (Figure 4g) alters at the 300°C heating step, causing a 'hedgehog' shaped Arai plot at higher temperatures. The low temperature component of this specimen is linear, but does not pass the *FRAC* requirement of 0.78. In addition, the Zijderveld diagram shows that the same low temperature component does not trend to the origin, resulting in a DANG value greater than 10°.

Hysteresis plots (Figures 4b, e, h) and first-order reversal curve diagrams (Figures 4c, f, i) suggest the presence of high coercivity, single-domain magnetic carriers. Specimens isl007b4 and isl009a2 have magnetization of remanence to magnetization of saturation (Mr/Ms) ratios of 0.31and 0.43, respectively, indicating a magnetic contribution from pseudo-single domain grains. Specimen isl007b3 has a high Mr/Ms ratio of 0.64 which has been previously observed in quenched seafloor basalts [*Gee and Kent*, 1995] and is shown to be the result of multi-axial single domain carriers [*Tauxe et al.*, 2002; *Mitra et al.*, 2011; *Williams et al.*, 2011]. FORC diagrams for each specimen show a distinct high coercivity band along the x-axis, indicative of single-domain magnetic material. This is to be expected considering the quenched volcanic material collected for this study is likely to be predominantly single-domain. Each specimen also has some low coercivity distributions along the y-axis frequently interpreted as multi-domain behavior, but could equally well be caused by a super-paramagnetic fraction. Interestingly, the specimen with the best behaved Arai plot, isl007b4 (Figure 5a), has the greatest degree of low coercivity behavior, suggesting that it is super paramagnetic, rather than multi-domain and underscoring the non-uniqueness of interpretations of hysteresis behavior. Conversely, specimen isl009a2 has a beautiful FORC diagram, but alters at a moderate temperature ($\sim 300^{\circ}$C).

These observations suggest that rock magnetic analyses are not necessarily good predictors of specimen behavior during paleointensity experiments.

In Figure 4 we looked at experimental results that represent most specimens in our data set. We now characterize less common experimental behaviors (Figure 5) that are found in relatively few specimens, but may pass our selection criteria, to ensure that all results accurately reflect the ancient field strength and to justify our specimen selection process. Specimens with low blocking temperatures may pass our selection requirements (e.g., islhhd2, Figure 5a), but might be the result of a secondary chemical remanent magnetization (CRM) or a viscous remnant magnetization (VRM), in which case the resulting paleointensity estimate would not be representative of the ancient field when the lava was emplaced. Several lava flows have specimens with low-blocking temperatures (like islhhd2) and when we compared those results to sister specimens with high blocking temperatures, we found that paleointensities for both specimen types are comparable, indicating that the observed low-blocking temperature is likely an original TRM. Specimen isl010a3 (Figure 5b) also has a small, low-blocking temperature component (or "hump") in the NRM-decay/TRM-growth curve and is accepted by the ThellierGUI selection routine, but the bulk of the magnetization is carried by higher temperature minerals. This low-temperature "hump" is likely a weathering feature due to the post-emplacement production of goethite and subsequent magnetization in the direction of the ambient magnetic field. A different example of a "two-humped" demagnetization that is not accepted is shown in Figure 5c. In this case, the low-blocking temperature component is between 300 and 400°C and is generally followed by signs of alteration during the heating experiment. These specimens often show different Arai slopes for each blocking temperature section, which results in the specimen failing *SCAT*. In some instances the change in slope is undetectable and the specimen will pass

all selection statistics, suggesting that alteration is minimal and the specimen can be included in site mean analysis.

Specimen isl009e3 (Figure 5d) represents a case of a physical mechanism for a magnetic signature with two directional components. Generally these types of behaviors fail the Thellier Gui selection process because the large *FRAC* requirement results in the MAD or DANG criteria exceeding their respective threshold values. Hyaloclastite sequences consist of volcaniclastic materials, like broken pillow fragments, that are deposited in layers. Prior to cooling completely through the magnetic blocking temperature, volcanic fragments may rotate, resulting in more than one directional component (see Zijderveld diagram in Figure 5d). For hyaloclastite specimens that exhibit a single rotation, we accept the high-blocking temperature component, regardless of *FRAC*, so long that the component passes all other selection statistics and there is no sign of experimental alteration in the Arai plot.

Figure 5e (specimen A-33d) shows a small viscous remanent magnetization component at low temperatures but the specimen alters at 300°C with no hope of passing any statistical requirements. Specimens exhibiting severe alteration were often removed from the paleointensity heating experiment prior to completion because they were sure to fail.

6. Iceland Paleointensity Results

Forty-four sites (out of 129, $\sim$35%) passed all site and specimen level selection criteria. Paleointensity results for each site are listed in Table 1 and median intensity estimates for different age groupings are listed in Table 3. We choose to calculate median values, and median absolute deviation (mad) uncertainties, rather than mean values, because we can not assume that our intensity data are normally distributed and the median statistic is less affected by large outliers. Individual specimen results, statistics, and measurement level data from this study can be found

in the MagIC database at http://earthref.org/MAGIC. Thirty-four sites are from the neovolcanic zone, and all but three are known to be Weichsel age (11-110 ka) or younger. Seven sites were collected in the Sida area, one of which, isl048/052, is the historic Laki eruption of 1783 C.E., and another, isl047 is the $\sim$4 ka Núpahraun lava flow. The other five Sida sites are estimated to be emplaced across the Matuyama-Gauss polarity boundary at 2.58 Ma [*Sæ mundsson and Jóhannesson*, 1980]. Three sites were successful from Skaftafell: isl020, isl041, and isl045. Site isl020 is Brunhes age [*Helgason and Duncan*, 2013], isl041 was emplaced between $3.20 - 3.35$ Ma [*Helgason and Duncan*, 2001], and isl045 between $2.35 - 2.59$ Ma [*Helgason and Duncan*, 2001]. No Núpakot area sites were successful.

One of our sites, the 1783 Laki lava flow (isl048/isl052) was also sampled by *Stanton et al.* [2011] and *Tanaka et al.* [2012] for paleointensity analysis. We collected material from glassy flow bottoms of these lavas (e.g., Figure 3d) while the other researchers drilled standard paleomagnetic holes into the massive interiors. *Stanton et al.* [2011] and *Tanaka et al.* [2012] both used the Coe variant of the Thellier-Thellier paleointensity method [*Coe*, 1967] with pTRM checks for alteration. *Tanaka et al.* [2012] also performed the Shaw intensity experiment [*Shaw*, 1974] on one sample per site. Average results and uncertainties for all three studies are listed in Table 4. The mean intensity value for our study and *Stanton et al.* [2011] are within one standard deviation of each other, but the *Tanaka et al.* [2012] mean barely exceeds the 1σ limit of our site. Our estimate has a within-site variance that is lower than *Stanton et al.* [2011] but slightly larger (1.2 μT) than *Tanaka et al.* [2012].

We plot the results for all 44 new Icelandic sites in Figure 6a, along with the median paleointensity (34.9 μT). Four sites are Holocene age (open circles) with a median intensity of 55.8 ± 15.6 μT. This value is equivalent to the present day Iceland field intensity of 52.5 μT

(calculated from igrf.py in the *PmagPy* software distribution) and significantly higher than the median strength for all older sites (gray circles, N=40, 33.1 ± 8.3 μT). The Weichsel, Brunhes and Matuyama/Gauss age intervals have equivalent median intensities of about 30 μT (Figure 6a, Table 3) and have similar site intensity distributions to each other.

Figure 6b is an enlargement of the Holocene and Weichsel age intervals ($0 - 110$ ka) showing the 33 youngest sites in Figure 6a (four, Holocene and 29 Weichsel). Median intensities for each interval are shown as dashed lines, emphasizing the high Holocene field strength and similarity between Weichsel intensity and that of older age intervals in Figure 6a. Within the Weichsel period, we were able to stratigraphically constrain five sites as Late Weichsel ($11 - 20$ ka) and four sites as Early Weichsel ($20 - 110$ ka), which have median paleointensity estimates of 33.0 $\pm$ 8.1 μT and 37.7 $\pm$ 4.9 μT, respectively. The 19 undifferentiated Weichsellian sites have a median intensity of 33.9 $\pm$ 5.8 μT and span the range of field estimates for the Early and Late periods, suggesting that these 18 sites are temporally distributed throughout the entire Weichsel period.

7. Discussion

7.1. Long-term Iceland Intensity

In Figure 7 we show the virtual axial dipole moments (VADMs) of our new Iceland sites (open and gray circles) and the PADM2M dipole moment model of *Ziegler et al.* [2011] (black line) which predicts the geomagnetic field strength for the last two million years. The median field strength for our Iceland data older than 11 ka (47.0 ZAm^2) is plotted as a dashed red line, and the mad uncertainty of the median ($\pm$ 11.6 ZAm^2) is represented by the shaded area. Recalculated VADMs of published high latitude sites from Jan Mayen (orange, *Cromwell et al.* [2013]) and McMurdo, Antarctica (blue, *Lawrence et al.* [2009]) are also plotted.

Brunhes age Iceland sites ($11 - 780$ ka, N=33) appear to agree with PADM2M, especially when taking into account the rather large age uncertainties for some lava flows. Median field strengths for both sets of data, however, show a substantially lower field in Iceland (46.0 ± 10.4 ZAm^2) compared to the PADM2M global model for the Brunhes (62.1 ZAm^2). Several Iceland sites of Weichsel age significantly underestimate PADM2M at the dipole low around 40 ka, suggesting that they might have been emplaced during the Laschamp excursion, and possibly influencing the lower overall field strength.

The median value of all non-Holocene paleointensity results (11 ka $-$ 3.3 Ma) are indistinguishable at the mad uncertainty level from the long-term geomagnetic field strength calculations of *Selkin and Tauxe* [2000] (46 ZAm^2), *Juarez et al.* [1998] and *Tauxe et al.* [2013] (42 ZAm^2, each), but remains substantially lower than the long-term estimate of *Tauxe and Yamazaki* [2007] (63 ZAm^2) and the median Brunhes value of PADM2M (62.1 ZAm^2). Long-term intensity calculations are based on compilations of global data and are dependent on the selection criteria used to select published results. *Juarez et al.* [1998], *Selkin and Tauxe* [2000] and *Tauxe et al.* [2013] based their estimates on data calculated using laboratory methods that checked for alteration, while *Tauxe and Yamazaki* [2007] and *Ziegler et al.* [2011] incorporated all available paleointensity data with no pre-selection requirements. The strict selection criteria used for our Icelandic data (including the use of pTRM checks) suggests that we have produced an accurate representation of field strength for the last few million years, and our agreement with the time-averaged intensity estimates of *Juarez et al.* [1998], *Selkin and Tauxe* [2000] and *Tauxe et al.* [2013] indicates that those calculations are reasonable.

The accuracy of long-term paleointensity estimates with no data selection requirements remains unclear. *Cromwell et al.* [2014b] addressed the accuracy of field estimates using bootstrap

simulations of all available published data from the 1960 Kilauea lava flow on the Big Island of Hawaii. The distribution of published results from the 1960 flow are biased high, relative to the expected intensity value, and *Cromwell et al.* [2014b] showed that this high bias will likely produce overestimates of the expected field, regardless of the number of samples used to calculate the mean value. Parametric bootstrap simulations of average field intensity at Hawaii, with full field vectors drawn from PSV model TK03 [*Tauxe and Kent*, 2004] and parameterized by the measured variability of 1960 flow results, result in an overestimate of the median TK03 intensity by 5-7 μT, or about 25% [*Cromwell et al.*, 2014b]. These results suggest that global paleointensity estimates which include results from all types of laboratory methodologies (e.g., *Tauxe and Yamazaki* [2007] and *Ziegler et al.* [2011]) overestimate the geomagnetic field strength, perhaps by as much as 25%. If a $\sim$60 ZAm^2 VADM is reduced by 25%, the resulting value would approximate the long-term field estimates calculated by *Juarez et al.* [1998], *Selkin and Tauxe* [2000], *Tauxe et al.* [2013], and our new Iceland results.

7.2. Reevaluation of Published Data

The strict selection criteria and experimental methodologies used in our study are not widely reproduced in the published literature and there are currently no data from comparable experiments at high latitudes. Accurate paleointensity results from both polar regions are required to sufficiently evaluate potential long-term non-dipole structures in the Arctic or Antarctic. In their Antarctica paper, *Lawrence et al.* [2009] applied similar site and specimen level selection statistics to those in this paper, but their threshold values for each statistic were much looser, especially the required fraction of NRM used for each specimen ($f_{vds} \geq 0.30$; see *Paterson et al.* [2014]) which is less than half of our required *FRAC* value ($\geq$ 0.78). Paleointensity estimates calculated from low percent fractions of NRM ($<\sim$40 to 50%) are often incorrect and are

usually biased to higher intensity values [*Chauvin et al.*, 2005] when authors select the steep, low temperature component in the Arai plot. The error resulting from low NRM fractions is often the result of poorly behaved intensity data, where alteration or concave-up Arai plots can produce NRM/TRM diagrams with variable slopes. Accurate specimen intensity estimates depend on linear NRM/TRM plots which should be constrained using objective selection statistics such as $\vec{k}'$ [*Paterson et al.*, 2014] or a combination of *SCAT* [*Shaar and Feinberg*, 2013] and a large NRM fraction. Mean site-level paleointensity estimates will have greater uncertainties and could be systematically biased (e.g., *Chauvin et al.* [2005]; *Paterson* [2011]; *Cromwell et al.* [2014b]) unless each specimen has a significant linear component and objective statistical controls.

We downloaded available high latitude measurement level data from McMurdo, Antarctic [*Lawrence et al.*, 2009] and Jan Mayen, Norway [*Cromwell et al.*, 2013] from the MagIC Database and applied our strict selection criteria to those data. From McMurdo, nine sites with radiometric ages younger than five million years passed our specimen and site level requirements (from youngest to oldest: mc218, mc35, mc217, mc109, mc142, mc15, mc147, mc120, mc117). One site from Jan Mayen also passed our criteria (JM012). Recalculated results from McMurdo (blue) and Jan Mayen (orange) are shown in Figure 7. The single Jan Mayen site and three McMurdo sites (mc218, mc35, mc217) are of comparable age to the Weichsel and Brunhes age Iceland results, and McMurdo site mc117 was emplaced at approximately the same time as the Icelandic Matuyama/Gauss sites. The remaining five McMurdo results are from the Matuyama epoch and do not overlap with any northern high latitude paleointensity data.

Similar field strength estimates should be expected from Jan Mayen and Iceland as they are separated by only $\sim$500 km. The VADM of site JM012 is equivalent to several Brunhes-age

457 Iceland sites and approximates the PADM2M dipole moment model. This single-site compari-
458 son of high latitude intensities supports some regional compatibility at Arctic latitudes, at least
459 during the Brunhes epoch.

460 In their original analysis of Antarctic intensity, *Lawrence et al.* [2009] observed a median
461 field strength of 38.0 ± 12.0 ZAm^2, from 41 sites, that was substantially lower than what was
462 predicted for that location based on published data (e.g. Figure 1). Our strict reevaluation of
463 the Antarctic collection produces an equivalent median field strength to *Lawrence et al.* [2009]
464 (34.3 vs 38.0 ZAm^2, respectively) but the variance of accepted sites is greatly reduced, with
465 mad uncertainty values of 3.6 ZAm^2 compared to 12.0 ZAm^2. Lower variance of the revised
466 Antarctic data supports our use of strict analytical controls as a means to improve the precision
467 of long-term paleointensity estimates.

468 Reinterpreted Antarctic VADMs are consistent with PADM2M and our Iceland results where
469 they have similar ages, however, the overall median strength of the Antarctic data (34.3 ± 3.6
470 ZAm^2) is lower than what we observe from Iceland sites older than 11 ka (47.0 ± 11.6 ZAm^2).
471 The Antarctic and Icelandic median values are distinct at the mad uncertainty level, and the rel-
472 atively reduced Antarctic field strength could be due to incomplete temporal comparisons; there
473 are five Matuyama-aged sites (mc109, mc142, mc15, mc147, mc120) with no Icelandic coun-
474 terparts. Both locations have average dipole moments that are lower than current values from
475 low- and mid-latitudes, and both are similar to the long-term geomagnetic strength estimates of
476 *Juarez et al.* [1998], *Selkin and Tauxe* [2000] and *Tauxe et al.* [2013]. These observations show
477 comparable field behaviors at high latitudes that may represent a more accurate depiction of
478 global field strength than do intensity data from lower latitudes, or it is possible that persistent
479 non-dipole field structures are found at high latitudes.

If we expand our discussion to include directional data from high latitudes we see that there may be some significant differences between the Arctic and Antarctic. Relatively high dispersion of virtual geomagnetic poles (VGPs) from Antarctic lava flows [*Lawrence et al.*, 2009] suggest a field structure that may be unique to high southern latitudes. Arctic paleodirectional data (n=37) for 0-2 [*Cromwell et al.*, 2013] and 0-10 Ma [*Cromwell et al.*, 2014a] show a reduced dispersion of VGPs relative to Antarctica (n=128), consistent with observations of directional scatter between hemispheres for modern and recent [*Korte et al.*, 2011] field evaluations. Unfiltered VGP dispersion values from high northern latitudes (e.g., *Udagawa et al.* [1999]; *Cromwell et al.* [2013]) generally agree with TK03 [*Tauxe and Kent*, 2004] (which assumes a geocentric axial dipole field), while dispersion estimates from Antarctica exceed the PSV predictions of TK03 and are better predicted by TK03-like models with a small $\bar{g}_2^0$ component [*Cromwell et al.*, 2014a]. Arctic PSV analysis and the correlation of Icelandic paleointensities with some long-term global averages, suggests that the geomagnetic field at high northern latitudes is consistent with a geocentric axial dipole for the last few million years. Time-averaged field structures in Antarctica, however, cannot be properly addressed at this time because there are still too few Antarctic paleointensity data that meet our selection criteria. The nine available results from McMurdo suggest that there may not be a significant difference between Antarctic and Arctic paleointensity but the paucity of southern hemisphere data means that the possibility of hemispheric asymmetry between the two regions can not be excluded.

8. Conclusions

We present a new collection of high-quality paleointensity results from Iceland. Thirty-seven sites were emplaced during the Brunhes epoch ($0 - 780$ ka) and 7 sites between $\sim 2.5 - 3.3$ Ma. We collected rapidly cooled material from subaerial and subglacial volcanic units across

Iceland and performed the IZZI-modified Thellier-Thellier experiment on all sites. The use of strict statistical criteria for site and specimen-level analyses produced paleointensity estimates with 1σ-uncertainties not exceeding 4 μT or 10% of the site mean.

Four Holocene sites (<11ka) have distinct intensities that approximate the present day field in Iceland (52.5 μT or 80 ZAm^2) and are substantially higher than the median strength of all older sites. The forty sites older than 11 ka have a median VADM of 47.0 $\pm$ 11.6 ZAm^2 (33.1 $\pm$ 8.3 μT) whch is indistinguishable at the mad uncertainty level to long-term geomagnetic field strength calculations by *Selkin and Tauxe* [2000] (46 ZAm^2), and *Juarez et al.* [1998] and *Tauxe et al.* [2013] (42 ZAm^2, each). Agreement between our median Iceland field estimate (excluding Holocene data) and global average estimates, suggest a GAD-like field intensity at high northern latitudes.

Reanalyzed high latitude intensity results (using our strict selection criteria) from Antarctica (N=9; *Lawrence et al.* [2009]) and Jan Mayen, Norway (n=1; *Cromwell et al.* [2013]) are generally consistent with our Icelandic data, although the median Antarctic field strength is slightly lower. Recent paleosecular variation studies observe different VGP dispersion values between the Arctic and Antarctic, suggesting asymmetric field structures at high latitude. Our paleointensity observations are inconclusive as there are too few reliable intensity results from Antarctica to properly evaluate hemispheric differences.

Acknowledgments. We would like to thank Leo Kristjánsson and Johann Helgason for their scientific expertise and hospitality in planning and executing this project. Thank you to David Hilton for generously providing many of the Icelandic samples, Karl Grönvold for his work in the field, and Kristján Saemundsson for clarifying several lava flow emplacement ages. We thank the staff at Vatnajökull National Park and Simon Berger Sigurgerrsson for allowing us

525 to access and sample many of the localities. Thanks to Jason Steindorf and Jesse Vavrek for
526 their hard work in the lab, and Erol Cromwell for preparing many of the samples. Thanks to
527 Ron Shaar, Hubert Staudigel and Jeff Gee for discussions leading to the success of this project.
528 And thank you to Cathy Constable, Jeff Gee, Dave Hilton, Catherine Johnson, Hubert Staudigel
529 and Tom Levy for their constructive reviews. This research was partially supported by NSF
530 EAR114840 to LT. All measurement data and results can be found online in the MagIC database
531 at http://earthref.org/MAGIC.

References

532 Banik, T., P. Wallace, A. Höskuldsson, C. Miller, C. Bacon, and D. Furbish (2014), Magma-
533 ice-sediment interactions and the origin of lava/hyaloclastite sequences in the Sída formation,
534 South Iceland, *Bull Volcanol, 76:785*, doi:10.1007/s00445-013-0785-3.

535 Barry, P., D. Hilton, E. Füri, S. Halldórsson, and K. Grönvold (2014), Carbon isotope and
536 abundance systematics of Icelandic geothermal gases, fluids and subglacial basalts with im-
537 plications for mantle plume-related CO_2 fluxes, *Geochemica et Cosmochimica Acta*, doi:
538 10.1016/j.gca.2014.02.038.

539 Bergh, S., and G. Sigvaldason (1991), Pleistocene mass-flow deposits of basaltic hyaloclastite
540 on a shallow submarine shelf, South Iceland, *Bulletin of Volcanology*, *53*, 597–611, doi:
541 10.1007/BF00493688.

542 Bjarnason, I., and H. Schmeling (2009), The lithosphere and asthenosphere of the Ice-
543 land hotspot from surface waves, *Geophys. J. Int.*, *178*(1), 394–418, doi:10.1111/j.1365-
544 246X.2009.04155.x.

Bowles, J., J. Gee, D. Kent, M. Perfit, S. Soule, and D. Fornari (2006), Paleointensity applications to timing and extent of eruptive activity, $9° - 10°$N East Pacific Rise, *Geochemistry Geophysics Geosystems*, *7*(6), doi:10.1029/2005GC001141.

Brown, M., J. Shaw, and A. Goguitchaichvili (2006), Microwave palaeointensity from the R3-N3 geomagetic field reversal, *Geophys. J. Int.*, *167*, 53–69, doi:10.1111/j.1365-246X.2006.03034.x.

Camps, P., B. Singer, C. Carvallo, A. Goguitchaichvili, G. Fanjat, and B. Allen (2011), The Kamikatsura event and the Matuyama-Brunhes reversal recorded in lavas from Tjörnes Peninsula, northern Iceland, *Earth and Planetary Science Letters*, *310*, doi: 10.1016/j.epsl.2011.07.026.

Cande, S., and D. Kent (1995), Revised calibration of the geomagnetic polarity timescale for the late Cretaceous and Cenozoic, *J. Geophys. Res.*, *100*, 6093–6095, doi:10.1029/94JB03098.

Chauvin, A., P. Roperch, and S. Levi (2005), Reliability of geomagnetic paleointensity data: the effects of the NRM fraction and concave-up behavior on paleointensity determinations by the Thellier method, *Physics of the Earth and Planetary Interiors*, *150*, 265–286.

Christensen, U., P. Olson, and G. Glatzmaier (1998), A dynamo model interpretation of the geomagnetic field structures, *Geophys. Res. Lett.*, *25*, 1565–1568.

Coe, R. (1967), Paleo-Intensities of the Earth's magnetic field determined from Tertiary and Quaternary rocks, *Journal of Geophysical Research*, *72*(12), 3247–3262.

Coe, R. S., S. Grommé, and E. A. Mankinen (1978), Geomagnetic paleointensities from radiocarbon-dated lava flows on Hawaii and the question of the Pacific nondipole low, *J. Geophys. Res.*, *83*, 1740–1756.

567 Cromwell, G., L. Tauxe, H. Staudigel, C. Constable, A. Koppers, and R.-B. Pedersen (2013),
568 In search of long term hemispheric asymmetry in the geomagnetic field: results from high
569 northern latitudes, *Geochemistry Geophysics Geosystems*, *14*(8), doi:10.1002/ggge.20174.

570 Cromwell, G., C. Johnson, L. Tauxe, C. Constable, and N. Jarboe (2014a), Paleosecular varia-
571 tion over the last 10 Ma from a new global dataset (PSV10): Evidence for long-term hemi-
572 spheric asymmetry, *Geochemistry Geophysics Geosystems, Submitted*.

573 Cromwell, G., L. Tauxe, H. Staudigel, and H. Ron (2014b), Paleointensity estimates from his-
574 toric and modern Hawaiian lava flows using basaltic volcanic glass as a primary source ma-
575 terial, *Physics of the Earth and Planetary Interiors, Submitted*.

576 Dunlop, D., and O. Özdemir (2001), Beyond Néel's theories: thermal demagnetization of
577 narrow-band partial thermoremanent magnetization, *Phys. Earth Planet. Int.*, *126*, 43–57.

578 Einarsson, P. (2008), Plate boundaries, rifts and transformations in Iceland, *Jökull*, *58*, 35–58.

579 Ferk, A., and R. Leonhardt (2009), The Laschamp geomagnetic field excursion recorded in
580 Icelandic lavas, *Physics of the Earth and Planetary Interiors*, *177*, 19–30.

581 Ferk, A., R. Leonhardt, K.-U. Hess, and D. Dingwell (2011), Paleointensities on 8ka obsidan
582 from Mayor Island, New Zealand, *Solid Earth*, *2*, 259–270, doi:10.5194/se-2-259-2011.

583 Füri, E., D. Hilton, S. Halldórsson, P. Barry, D. Hahm, T. Fischer, and K. Grönvold (2010),
584 Apparent decoupling of the He and Ne isotope systematics of the Icelandic mantle: The
585 role of He depletion, melt mixing, degassing fractionation and air interaction, *Geochemica et*
586 *Cosmochimica Acta*, *74*, 3307–3332, doi:10.1016/j.gca.2010.03.023.

587 Gee, J., and D. Kent (1995), Magnetic hysteresis in young mid-ocean ridge basalts: dominant
588 cubic anisotropy, *Geophysical Research Letters*, *22*(5), 551–554, doi:10.1029/95GL00263.

589 Geirsdóttir, A., and J. Eiríksson (1994), Growth of Intermittent Ice Sheet in Iceland during the
590 Late Pliocene and Early Pleistocene, *Quaternary Research*, *42*, 115–130.
591 Glatzmaier, A., R. S. Coe, L. Hongre, and P. Roberts (1999), The role of the Earth's mantle in
592 controlling the frequency of geomagnetic reversals, *Nature*, *401*, 885–890.
593 Goguitchaichvili, A., M. Prevot, and P. Camps (1999), No evidence for strong fields during the
594 R3-N3 Iceland geomagnetic reversal, *Earth and Planetary Science Letters*, *167*, 15–34.
595 Gubbins, D., A. Jones, and C. Finlay (2006), Fall in the Earth's magnetic field and implications
596 for the geodynamo, *Science*, *312*, 900–902, doi:10.1126/science.1124855.
597 Guillou, H., B. van Vliet-Lanoë, A. Gudmundsson, and S. Nomade (2010), New unspiked K-
598 Ar ages of Quaternary sub-glacial and sub-aerial volcanic activity in Iceland, *Quaternary*
599 *Geochronology*, *5*, 10–19, doi:10.1016/j.quageo.2009.08.007.
600 Harrison, R., and J. Feinberg (2008), An improved algorithm for calculating first-order reversal
601 curve distributions using locally weighted regression smoothing, *Geochemistry Geophysics*
602 *Geosystems*, *9*, doi:10.1029/2008GC001987.
603 Helgason, J. (2007), Skaftafell Bedrock Geology, 1:25.000.
604 Helgason, J., and R. Duncan (2001), Glacial-interglacial history of the Skaftafell
605 region, southeast Iceland, 0-5 Ma, *Geology*, *29*(2), 179–182, doi:10.1130/0091-
606 7613(2001)029<0179:GIHOTS>2.0.CO;2.
607 Helgason, J., and R. Duncan (2013), Stratigraphy, ^{40}Ar-^{39}Ar dating and erosional history of
608 Svínafell, SE-Iceland, *Jökull*, *63*, 33–54.
609 Herrero-Bervera, E., and J. P. Valet (2009), Testing determinations of absolute paleointensity
610 from the 1955 and 1960 Hawaiian flows, *Earth and Planetary Science Letters*, *287*, 420–433.

Hjartarson, A. (1994), Environmental changes in Iceland following the Great Thjórsá Lava Eruption 7800^{14}C years BP, *In Stötter, J., Wilhelm F. (Eds.), Environmental Change in Iceland. Münchener Geographische Abhandlungen, Reihe B Munchen*, pp. 147–155.

Hulot, G., C. Eymin, B. Langlais, M. Mandea, and N. Olsen (2002), Small-scale structure of the geodynamo inferred from Oersted and Magsat satellite data, *Nature*, *416*(6881), 620–623, doi:10.1038/416620a.

Jackson, A., A. R. T. Jonkers, and M. R. Walker (2000), Four centuries of geomagnetic secular variation from historical records, *Phil Trans Roy Soc London, Series A*, *358*(1768), 957–990.

Jakobsson, S., K. Jonasson, and I. Sigurdsson (2008), The three igenous rock series of Iceland, *Jökull*, *58*, 117–138.

Jicha, B., L. Kristjánsson, M. Brown, B. Singer, B. Beard, and C. Johnson (2011), New age for the Skálamaelifell excursion and identification of a global geomagnetic event in the late Brunhes chron, *Earth and Planetary Science Letters*, *310*, 509–517, doi: 10.1016/j.epsl.2011.08.007.

Jóhannesson, H. (1983), Fródleiksmolar um Grænalón og nágrenni (in Icelandic), *Náttúrufrædingurinn*, *52*, 86–101.

Jóhannesson, H. (1985), Um endasleppu hraunin undir Eyjafjöllum og jökla sídasta jökulskeids (in Icelandic), *Jökull*, *35*, 51–60.

Jóhannesson, H., and S. Einarsson (1988), Krísuvíkureldar I: Aldur Ögmundarhrauns og midaldalagsins (The Krýsuvík fires I: age of the Ögmundarhraun lava and the Medieval tephra layer), *Jökull*, *38*, 103–109.

Jóhannesson, H., and K. Sæ mundsson (2009), Geological Map of Iceland. 1:600 000. Bedrock Geology, *Icelandic Institute of Natural History, Reykjavik (1st Edition)*.

Johnson, C. L., and C. Constable (1996), Palaeosecular variation recorded by lava flows over the past five million years, *Phil Trans Roy Soc London, Series A*, *354*, 89–141, doi: 10.1098/rsta.1996.0004.

Jónsson, J. (1974), Óbrinnishólar (In Icelandic), *Náttúrufrædingurinn*, *44*, 109–119.

Juarez, M., L. Tauxe, J. Gee, and T. Pick (1998), The intensity of the Earth's magnetic field over the past 160 million years, *Nature*, *394*(6696), 878–881.

Kelly, P., and D. Gubbins (1997), The geomagnetic field over the past 5 million years, *Geophys. J. Int.*, *128*, 315–330.

Kirschvink, J. L. (1980), The least-squares line and plane and the analysis of paleomagnetic data, *Geophys. Jour. Roy. Astron. Soc.*, *62*, 699–718, doi: 10.1111/j.1365246X.1980.tb02601.x.

Korte, M., C. Constable, F. Donadini, and R. Holme (2011), Reconstructing the Holocene geomagnetic field, *Earth and Planetary Science Letters*, *312*, 497–505, doi: 10.1016/j.epsl.2011.10.031.

Kristjánsson, L. (2010), Paleomagnetic observations at three locations in the Pleistocene lava sequences of southwest and south Iceland, *Jökull*, *60*, 149–164.

Kristjánsson, L. (2013), Analyses of primary remanence vector data from a large collection of lava flows: towards improved methodology in paleo-geomagnetism, *Stud. Geophys. Geod.*, *57*(4), 543–564, doi:10.1007/s11200-012-0480-4.

Kristjánsson, L., I. Fridleifsson, and N. Watkins (1980), Stratigraphy and Paleomagnetism of the Esja, Eyrarfjall and Akrafjall Mountains, SW-Iceland, *J. Geophys*, *47*, 31–42.

Kristjánsson, L., H. Jóhannesson, J. Eiríksson, and A. Gudmundsson (1988), Brunhes-Matuyama paleomagnetism in three lava sections in Iceland, *Canadian Journal of Earth Sci-*

ence, *25*, 215–225, doi:10.1139/e88-024.

Kristjánsson, L., R. Duncan, and A. Gudmundsson (1998), Stratigraphy, palaeomagnetism and age of volcanics in the upper regions of Thórsádalur valley, central southern Iceland, *Boreas*, *27*.

Lawley, E. (1970), The intensity of the geomagnetic field in Iceland during Neogene polarity transitions and systematic deviations, *Earth and Planetary Science Letters*, *10*, 145–149.

Lawrence, K. P., L. Tauxe, H. Staudigel, C. Constable, A. Koppers, W. C. McIntosh, and C. L. Johnson (2009), Paleomagnetic field properties near the southern hemisphere tangent cylinder, *Geochem. Geophys. Geosyst.*, *10*, *Q01005*, doi:10.1029/2008GC00,207.

Levi, S., H. Audunsson, R. A. Duncan, L. Kristjansson, P. Y. Gillot, and S. Jakobsson (1990), Late Pleistocene geomagnetic excursion in Icelandic lavas: confirmation of the Laschamp excursion, *Earth and Planetary Science Letters*, *96*, 443–457.

Licciardi, J., M. Kurz, and J. Curtice (2007), Glacial and volcanic history of Icelandic table mountains from cosmogenic He-3 exposure ages, *Quaternary Science Reviews*, *26*(11-12), 1529–1546, doi:10.1016/j.quascirev.2007.02.016.

Love, J., and C. Constable (2003), Gaussian statistics for palaeomagnetic vectors, *Geophys. J. Int.*, *152*, 515–565.

Macpherson, C., D. Hilton, J. Day, D. Lowry, and K. Grönvold (2005), High-^{3}He/^{4}He, depleted mantle and low-δ^{18}O, recycled oceanic lithosphere in the source of central Iceland magmatism, *Earth and Planetary Science Letters*, *233*(3-4), 411–427, doi: 10.1016/j.epsl.2005.02.037.

Marshall, M., A. Chauvin, and N. Bonhommet (1988), Preliminary paleointensity measurements and detailed magnetic analyses of basalts from the Skalamaelifel excursion, Southwest

Iceland, *Journal of Geophysical Research*, *93*, 11,681–11,698.

McDougall, I., K. Saemundsson, H. Johannesson, N. Watkins, and L. Kristjánsson (1977), Extension of the geomagnetic polarity time scale to 5.5 m.y.: K-Ar dating, geological and paleomagnetic study of a 3,500-m lava succession in western Iceland, *Bull. Geol. Soc. Am.*, *88*, 1–15, doi:10.1130/0016-7606(1977)88<1:EOTGPT>2.0.CO;2.

McDougall, I., L. Kristjánsson, and K. Saemundsson (1984), Magnetostratigraphy and geochronology of Northwest iceland, *J. Geophys. Res.*, *89*, 7029–7060, doi: 10.1029/JB089iB08p07029.

Mitra, R., L. Tauxe, and J. Gee (2011), Detecting uniaxial single domain grains with a modified IRM technique, *Geophysical Journal International*, doi:10.1111/j.1365-246X.2011.05224.x.

Nagata, T., Y. Arai, and K. Momose (1963), Secular variation of the geomagnetic total force during the last 5000 years, *J. Geophys. Res*, *68*, 5277–5282.

Olson, P., and J. Aurnou (1999), A polar vortex in the Earth's core, *Nature*, *402*(6758), 170–173, doi:10.1038/46017.

Paterson, G. (2011), A simple test for the presence of multidomain behavior during paleointensity experiments, *Journal of Geophysical Research*, *116*, B10,104.

Paterson, G., L. Tauxe, A. Biggin, R. Shaar, and L. Jonestrask (2014), On improving the selection of Thellier-type paleointensity data, *Geochemistry Geophysics Geosystems*, *15*, 1180–1192, doi:10.1002/2013GC005135.

Pick, T., and L. Tauxe (1993), Holocene Paleointensities: Thellier Experiments on Submarine Basaltic Glass From the East Pacific Rise, *Jour. Geophys. Res.*, *98*(B10), 17,949–17,964, doi:10.1038/366238a0.

Roberts, N., and J. Shaw (1984), The relationship between the magnitude and direction of the geomagnetic field during the Late Tertiary in Eastern Iceland, *Geophys. J. Roy. Astron. Soc*, *76*, 637–651.

Sæ mundsson, K., and H. Jóhannesson (1980), Jardfrædirannsóknir á Fljótshverfis- og Sídumannaafréttum (In Icelandic), *Geological Society of Iceland Meeting. Reykjavík, Iceland.*

Saemundsson, K., and H. Noll (1974), K/Ar ages of rocks from Husafell, Western Iceland and the development of the Husafell central volcano, *Jökull*, *24*, 40–59.

Saemundsson, K., H. Jóhannesson, A. Hjartarson, S. Kristinsson, and M. Sigurgeirsson (2010), Geological Map of Southwest Iceland, 1:100 000, *Iceland GeoSurvey*.

Schweitzer, C., and H. Soffel (1980), Palaeointensity Measurements on Postglacial Lavas From Iceland, *Journal of Geophysics*, *47*, 57–60.

Selkin, P., and L. Tauxe (2000), Long-term variations in palaeointensity, *Phil. Trans. R. Soc. Lond.*, *358*, 1065–1088.

Senanayake, W., M. McElhinny, and P. McFadden (1982), Comparison between the Thelliers' and Shaw's Palaeointensity Methods Using Basalts Less than 5 Million Years Old, *J. Geomag. Geoelectr.*, *34*(141-161).

Shaar, R., and J. Feinberg (2013), Rock magnetic properties of dendrites: insights from MFM imaging and implications for paleomagnetic studies, *Geochemistry Geophysics Geosystems*, *14*(2), doi:10.1002/ggge.20053.

Shaar, R., and L. Tauxe (2013), Thellier Gui: An integrated tool for analyzing data from Thellier-type experiments, *Geochemistry Geophysics Geosystems*, *14*(3), doi: 10.1002/ggge.20062.

Shaw, J. (1974), A new method of determining the magnitude of the paleomagnetic field application to five historic lavas and five archeological samples, *Geophys. J. R. Astron. Soc.*, *39*, 133–141.

Shaw, J. (1975), Strong Geomagnetic Fields during a single Icelandic Polarity Transition, *Geophys. J. R. Astron. Soc.*, *40*, 345–350, doi:10.1111/j.1365-246X.1975.tb04136.x.

Sinton, J., K. Grönvold, and K. Saemundsson (2005), Postglacial eruptive history of the Western Volcanic Zone, Iceland, *Geochemistry Geophysics Geosystems*, *6*, doi: 10.1029/2005GC001021.

Stanton, T., P. Riisager, M. Knudsen, and T. Thordarson (2011), New palaeointensity data from Holocene Icelandic lavas, *Physics of the Earth and Planetary Interiors*, *186*, 1–10, doi:doi:10.1016/j.pepi.2011.01.006.

Tanaka, H., M. Kono, and H. Uchimura (1995a), Some global features of palaeointensity in geological time, *Geophys. J. Int.*, *120*, 97–102.

Tanaka, H., M. Kono, and S. Kaneko (1995b), Paleosecular variation of Direction and Intensity from Two Pliocene-Pleistocene Lava Sections in Southwestern Iceland, *J. Geomag. Geoelectr.*, *47*, 89–102.

Tanaka, H., Y. Hashimoto, and N. Morita (2012), Palaeointensity determinations from historical and Holocene basalt lavas in Iceland, *Geophysical Journal International*, *189*(2), 833–845, doi:10.1111/j.1365-246X.2012.05412.x.

Tauxe, L. (2006), Long-term trends in paleointensity: The contribution of DSDP/ODP submarine basaltic glass collections, *Physics of the Earth and Planetary Interiors*, *156*, 223–241, doi:10.1016/j.pepi.2005.03.022.

747 Tauxe, L., and D. V. Kent (2004), A simplified statistical model for the geomagnetic field and
748 the detection of shallow bias in paleomagnetic inclinations: Was the ancient magnetic field
749 dipolar?, in *Timescales of the Paleomagnetic Field*, vol. 145, edited by e. a. Channell, J.E.T.,
750 pp. 101–116, American Geophysical Union, Washington, D.C.

751 Tauxe, L., and H. Staudigel (2004), Strength of the geomagnetic field in the Cretaceous Normal
752 Superchron: New data from submarine basaltic glass of the Troodos Ophiolite, *Geochem.*
753 *Geophys. Geosyst.*, *5*(2), doi:10.1029/2003GC000635.

754 Tauxe, L., and T. Yamazaki (2007), Paleointensities, in *Geomagnetism*, *Treatise on Geophysics*,
755 vol. 5, edited by M. Kono, pp. 509–563, doi:10.1016/B978–044452,748–6/00,098–5, Else-
756 vier.

757 Tauxe, L., H. Bertram, and C. Seberino (2002), Physical interpretation of hysteresis loops:
758 Micromagnetic modeling of fine particle magnetite, *Geochemistry Geophysics Geosystems*,
759 *3*(10), doi:10.1029/2001GC000241.

760 Tauxe, L., J. Gee, M. Steiner, and H. Staudigel (2013), Paleointensity results from the Juras-
761 sic: New constraints from submarine basaltic glasses of ODP Site 801C, *Geochemistry Geo-*
762 *physics Geosystems*, *14*(10), doi:10.1002/ggge/20282.

763 Thordarson, T., and A. Hoskuldsson (2008), Postglacial volcanism in Iceland, *Jökull*, *58*, 197–
764 228.

765 Udagawa, S., H. Kitagawa, A. Gudmundsson, O. Hiroi, T. Koyaguchi, H. Tanaka, L. Krist-
766 jansson, and M. Kono (1999), Age and magnetism of lavas in Jökuldalur area, Eastern
767 Iceland: Gilsá event revisited, *Phys. Earth Planet. Int.*, *115*, 147–171, doi:10.1016/S0031-
768 9201(99)00073-4.

769 Walker, G. (1959), Geology of the Reydarfjördur area, eastern Iceland, *Quart. J. Geol. Soc.*
770 *London*, *114*, 367–391.
771 Watkins, N., and G. Walker (1977), Magnetostratigraphy of Eastern Iceland, *Am. J. Sci.*, *277*,
772 513–584.
773 Williams, W., A. Muxworthy, and M. Evans (2011), A micromagnetic investigation of magnetite
774 grains in the form of Platonic polyhedra with surface roughness, *Geochemistry Geophysics*
775 *Geosystems*, *12*(10), doi:10.1029/2011GC003560.
776 Ziegler, L., C. Constable, C. L. Johnson, and L. Tauxe (2011), PADM2M: a penalized maximum
777 likelihood model of the 0-2 Ma palaeomagnetic axial dipole moment, *Geophys. J. Int.*, doi:
778 10.1111/j.1365-246X.2010.04905.x.

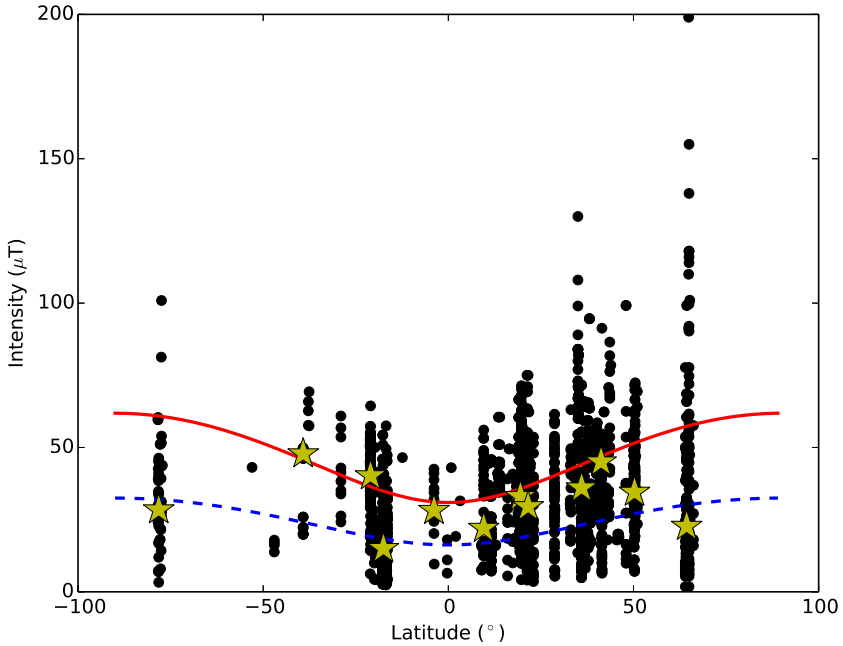

Figure 1. Site level paleointensity data (method code of LP-PI-TRM), with standard deviations $\leq$15% or $\leq$5 μT downloaded from the MagIC database (http://earthref.org/MagIC) from the last 5 Myr. Data are plotted against latitude and median values for 10° bins are shown as yellow stars. Predicted values for dipole moments of 80 (present field) and 42 ZAm^2 [*Juarez et al.*, 1998; *Tauxe et al.*, 2013] are shown as solid red and dashed blue lines respectively.

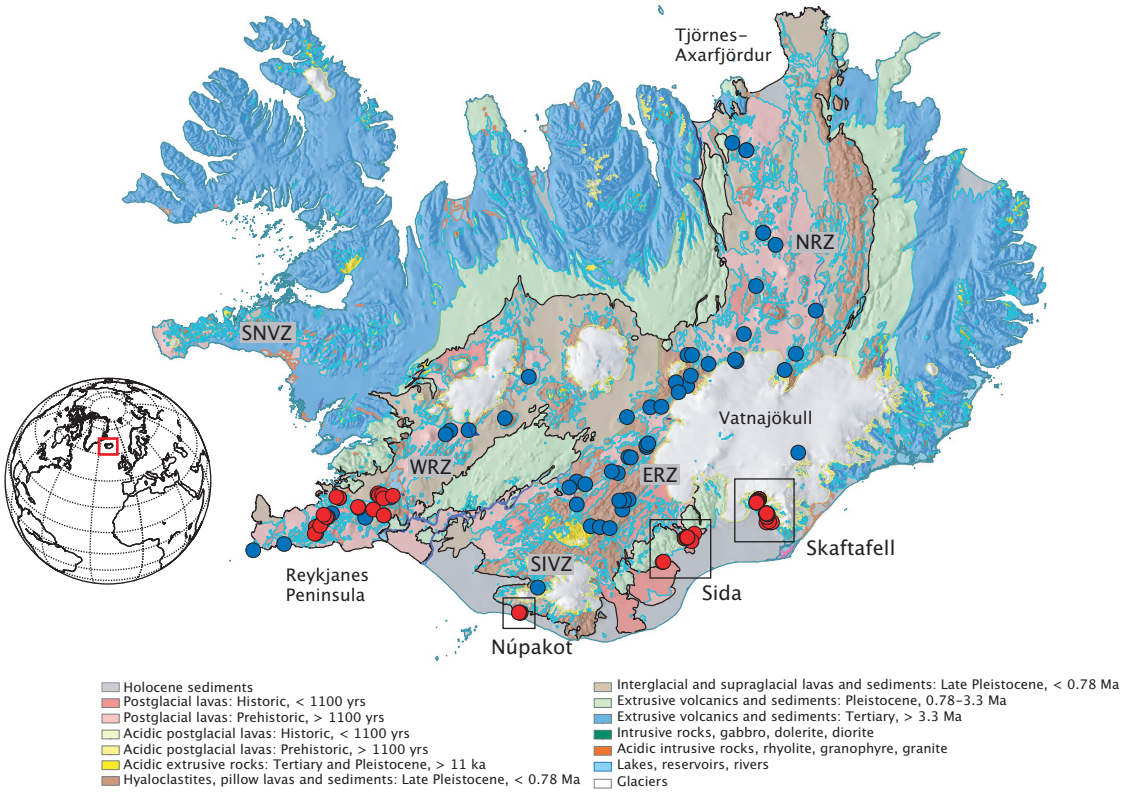

Figure 2. Geologic map of Iceland showing regional volcanic systems. The Western (WRZ), Eastern (ERZ) and Northern (NRZ) axial rift zones are labeled, as well as the off-axis South Iceland (SIVZ) and Snaefellsness (SNVZ) volcanic zones. The neovolcanic zone (<780 ka) is outlined in black and is our largest sampling region. Núpakot, Sida, and Skaftafell are sampling areas specific to the 2012 field expedition, comprising geologic formations older than 780 ka. Site locations from the pre-2006 and 2008 field seasons are plotted in blue ($N = 63$) and the 2012 sites are in red ($N = 66$). Geology derived from *Jóhannesson and Sæ mundsson* [2009] and the Icelandic Institute of Natural History.

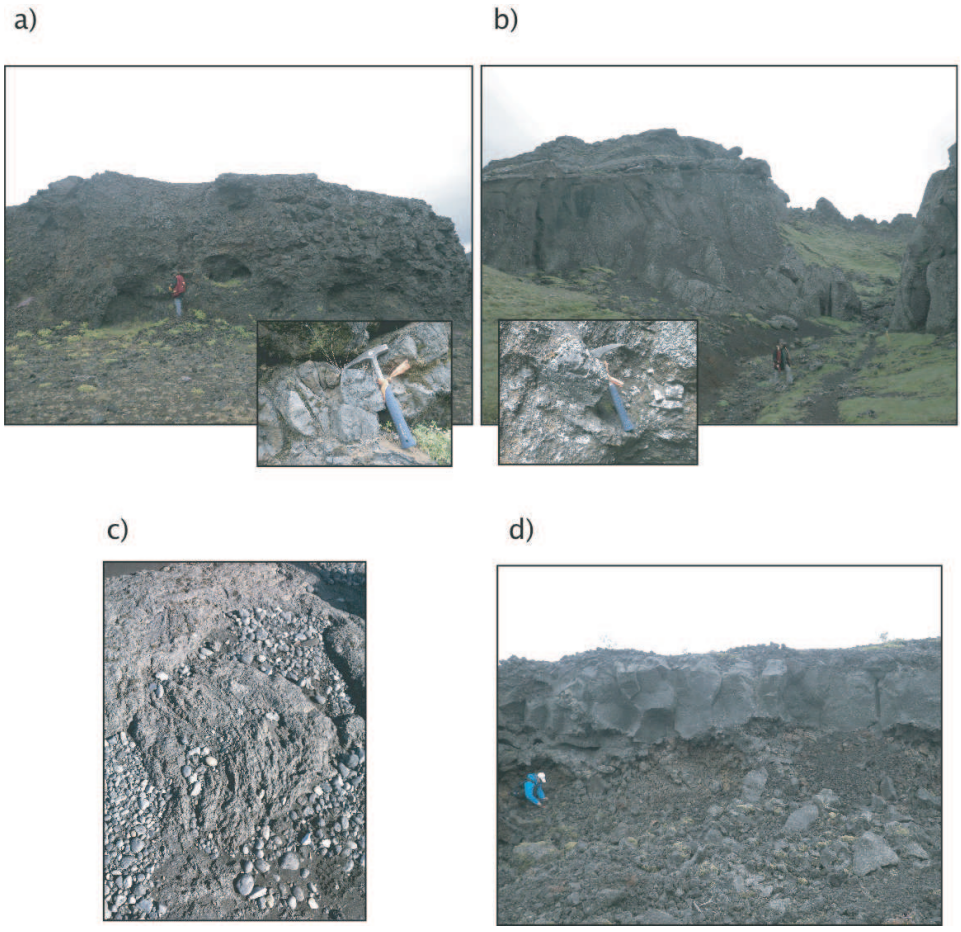

Figure 3. Photos of typical sample localities. a) Pillow basalt outcrop (isl004). b) Hyaloclastite sequence (isl009). c) Pahoehoe flow top (isl048). d) Subaerial lava flow bottom (isl066).

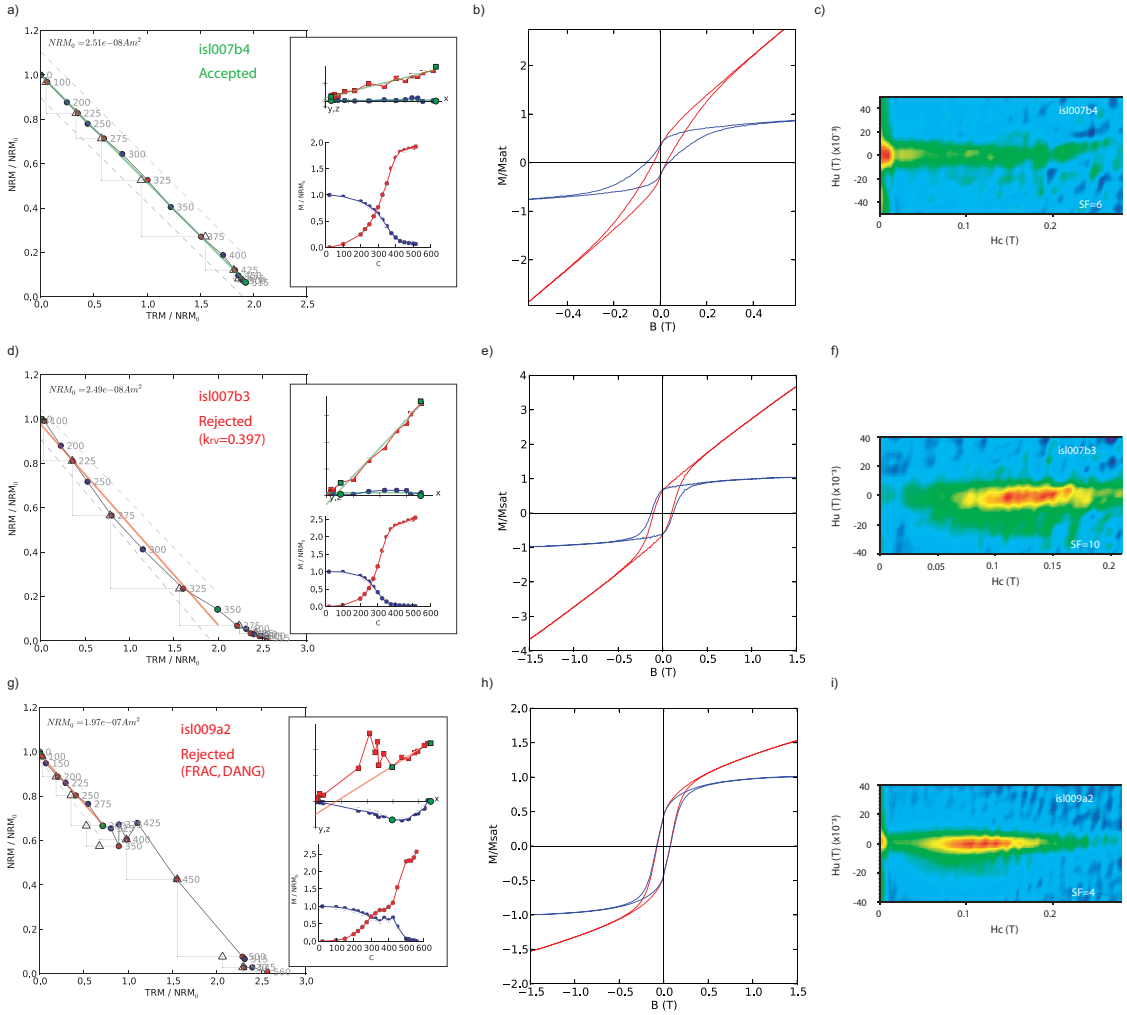

Figure 4. Representative paleointensity and rock magnetic results. Arai plots (with inset Zijderveld diagrams and NRM-decay/TRM-growth curves) are plotted in a, d, g. Temperature values for Arai plots are listed in degree Celcius. pTRM checks are shown as open triangles, zero-field/in-field (ZI) temperature steps shown as red dots and IZ steps shown in blue. The green line is the least-squares component for selected temperature steps. X-axes in the Zijderveld diagrams are rotated to the specimen declination. NRM-decay curves are shown in blue, TRM-growth curves in red. Hysteresis loops (b, e, h) show the raw hysteresis data in red and the resulting loop after paramagnetic slope corrections in blue. First-order reversal curve (FORC) diagrams are plotted in c, f, and i, and SF is the smoothing factor applied to each FORC.

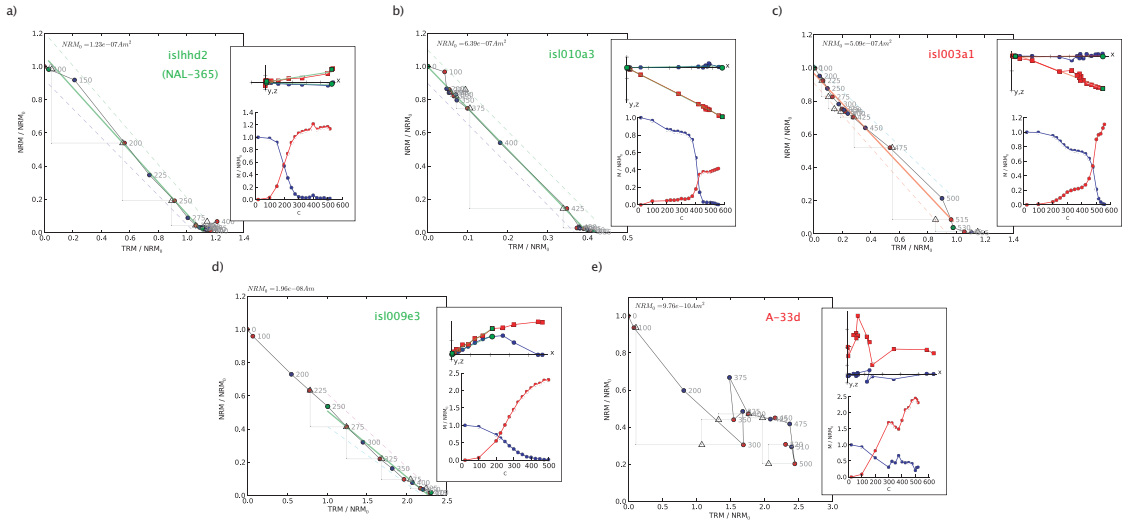

Figure 5. Representative experimental behaviors for accepted (a, b, d) and rejected (c, e) specimens. Arai plots with inset Zijderveld diagrams and NRM-decay/TRM-growth curves are plotted for each specimen. The x-axis of the Zijderveld diagrams are rotated to the specimen declination.

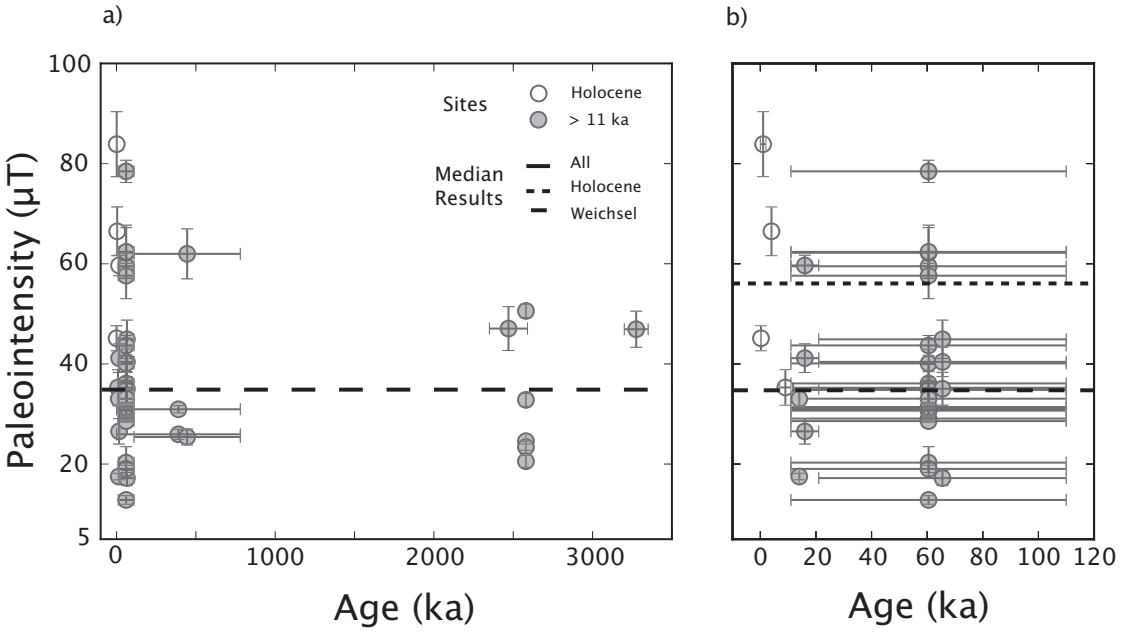

Figure 6. Paleointensity results (with 1-σ error bars) plotted with age for successful sites. Age estimates and uncertainties are listed in Tables 1. a) All sites. b) Enlargement of Holocene and Weichsel-aged sites ($0 - 110$ ka).

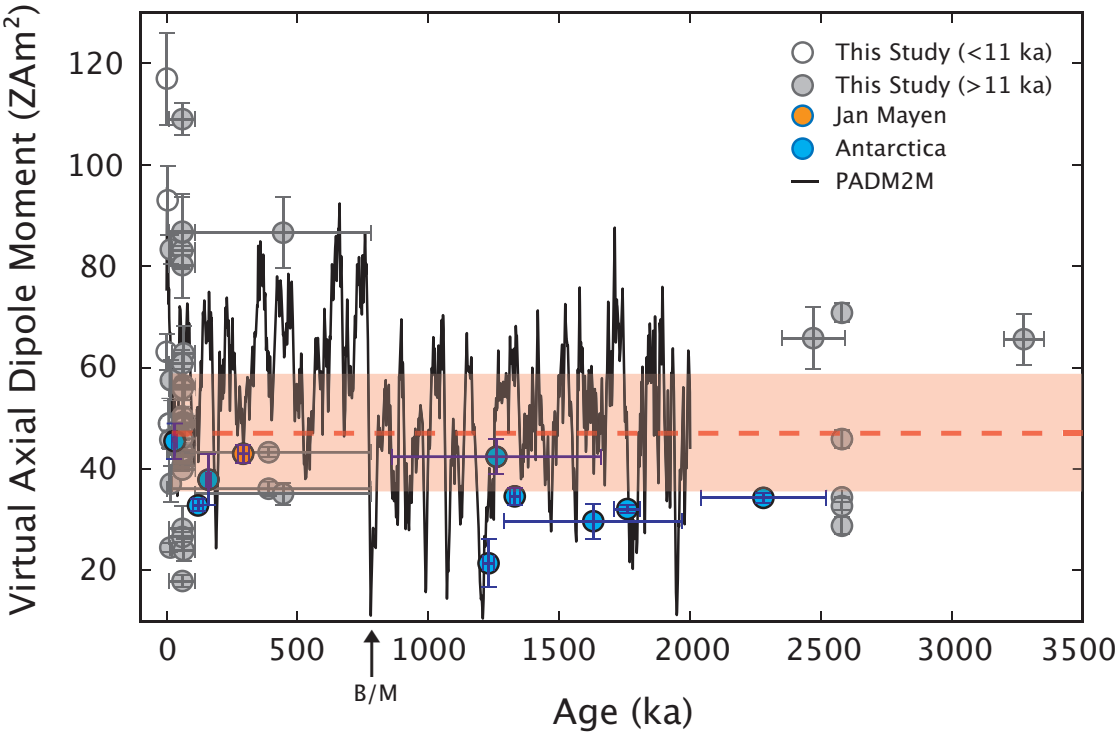

Figure 7. VADM site estimates for Holocene (open) and older (gray) Icelandic sites. High latitude sites from Jan Mayen (orange, *Cromwell et al.* [2013]) and Antarctica (blue, *Lawrence et al.* [2009]) pass our strict selection criteria. PADM2M dipole moment model for 0-2 Ma [*Ziegler et al.*, 2011] shown in black. The dashed red line is the median VADM for all Icelandic sites older than 11 ka (47.0 ZAm^2), and the shaded area reflects the median absolute deviation ($\pm$11.6 ZAm^2). The Brunhes/Matuyama boundary (B/M) is marked at 780 ka.

Table 1: Average paleointensity results and location information for all Iceland sites. Site column lists the primary site names used in this study, Alt. Names are corresponding labels for the same volcanic unit from other publications. Region names are the sampling areas shown in Figure 2. Age estimates are based on descriptions in Section 3, *Sample Collection*. nn is the number of successful specimens per site. B_F is the average field strength, $B_{F\sigma}$ is the standard deviation of the average site estimate, and $B_{F\sigma}$ % is the percent difference. VADM and $VADM_\sigma$ are the average virtual axial dipole moment estimates and the standard deviation of the site mean, respectively. Additional references: *a-This study, b-Helgason and Duncan* [2001], *c-Stanton et al.* [2011], *d-Tanaka et al.* [2012], *e-Füri et al.* [2010], *f-Bergh and Sigvaldason* [1991], *g-Saemundsson et al.* [2010], *h-Helgason and Duncan* [2013], *i-Jóhannesson* [1983], *j-Thordarson and Hoskuldsson* [2008], *k-Sæ mundsson and Jóhannesson* [1980], *l-Kristjánsson et al.* [1988], *m-Sinton et al.* [2005], *n-Jóhannesson and Einarsson* [1988], *o-Licciardi et al.* [2007], *p-Guillou et al.* [2010], *q-Jóhannesson and Sæ mundsson* [2009].

Site	Alt. Name	Region	Location	Lat (°N)	Lon (°E)	Sample Type	Age	Age Ref.	nn	B_F	$B_{F\sigma}$	$B_{F\sigma}$ %	VADM	$VADM_\sigma$
isl001		WRZ	Draugahlidar	64.05337	-21.53227	pillow margin	Early Weichsel	*g*						
isl002		WRZ	Stakur	63.99739	-21.88661	pillow margin	Early Weichsel	*g*	12	40.41	2.95	7.29	5.65E+22	4.12E+21
isl003		WRZ	Nordlingaháls	63.94583	-22.00179	hyaloclastite	Early Weichsel	*g*						
isl004	KLE-1[a,e]	WRZ	Kleifarvatn	63.91118	-22.01106	pillow margin	Late Weichsel	*g*						
isl005		WRZ	Blesaflöt	63.95283	-21.95390	flow top	Early Brunhes	*g*						
isl006		WRZ	Stakur	63.99659	-21.88837	pillow margin	Early Weichsel	*g*	Results combined with isl002					
isl007		WRZ	Dyrafjöll	64.12054	-21.31619	hyaloclastite	Late Weichsel	*g*	5	17.51	0.65	3.73	2.45E+22	9.08E+20
isl008		WRZ	Dyrafjöll	64.12514	-21.30965	hyaloclastite	Early Weichsel	*g*						
isl009		WRZ	Dyrafjöll	64.11542	-21.29806	hyaloclastite	Early Weichsel	*g*	5	17.2	1.5	8.5	2.40E+22	2.10E+21
isl010		WRZ	Nesjavellir	64.11833	-21.26096	agglutinate	$<$ 2 ka	*g*	4	83.88	6.49	7.73	1.17E+23	9.06E+21
isl011	NES-1[a,e]	WRZ	Nesjavellir	64.10016	-21.24725	pillow margin	Late Weichsel	*g*	10	26.53	2.54	9.56	3.71E+22	3.55E+21
isl012	OLF-1[a,e]	WRZ	Ölfusvatnsfjöll	64.11546	-21.14066	pillow margin	Early Weichsel	*g*	6	35.04	3.28	9.36	4.89E+22	4.58E+21
isl013	SKARD-1[ae]	WRZ	Skardsmýrarfjall	64.04375	-21.35805	pillow margin	Late Weichsel	*g*	14	41.15	2.86	6.96	5.75E+22	4.00E+21
isl014		WRZ	Hverakjálki	64.01681	-21.23582	hyaloclastite	Early Brunhes	*g*						
isl014b		WRZ	Hverakjálki	64.01681	-21.23582	crystalline flow	Early Brunhes	*g*	3	61.98	4.99	8.06	8.66E+22	6.97E+21
isl015	SV13[b]	Skaftafell	Svinafell	63.98347	-16.84140	pillow margin/dike margin	$>$ 0.757 Ma	*b*						
isl016	SV14[b]	Skaftafell	Svinafell	63.98148	-16.83116	dike margin	$>$ 0.757 Ma	*b*						
isl017	SV14[b]	Skaftafell	Svinafell	63.98148	-16.83116	aa flow bottom	$>$ 0.757 Ma	*b*						
isl018	SV21[b]	Skaftafell	Svinafell	63.98137	-16.87985	flow bottom, hyaloclastite	0.65 Ma	*b*						
isl019	SV23[b]	Skaftafell	Svinafell	63.98146	-16.81626	pillow margin, flow top	$<$ 0.65 Ma	*b*						
isl020	SV12[b]	Skaftafell	Svinafell	63.98666	-16.84952	pillow margin	$<$ 0.780 Ma	*h*	6	30.94	0.72	2.34	4.33E+22	1.01E+21
isl021		Skaftafell	Skaftafellsfjöll	64.09930	-16.95398	dike margin								
isl022		Skaftafell	Skaftafellsfjöll	64.09930	-16.95398	dike margin								
isl023	JM10[b]	Skaftafell	Skaftafellsfjöll	64.09930	-16.95398	hyaloclastite	Matuyama	*b*						
isl024	JM10[b]	Skaftafell	Skaftafellsfjöll	64.09921	-16.95598	pillow margin	Matuyama	*b*						
isl025		Skaftafell	Skaftafellsfjöll	64.09046	-16.96967	dike margin								
isl026	JM8A[b]	Skaftafell	Skaftafellsfjöll	64.09050	-16.96996	hyaloclastite	Matuyama/Gauss	*b*						
isl027	JM8C[b]	Skaftafell	Skaftafellsfjöll	64.09065	-16.97126	flow bottom	Lower Matuyama	*b*						
isl028	JM8C[b]	Skaftafell	Skaftafellsfjöll	64.09040	-16.97148	hyaloclastite	Lower Matuyama	*b*						
isl029		Skaftafell	Skaftafellsfjöll	64.09040	-16.97148	dike margin								
isl030		Skaftafell	Skaftafellsfjöll	64.09200	-16.97715	dike margin								
isl031		Skaftafell	Skaftafellsfjöll	64.09194	-16.97571	dike margin								
isl032	JM7B[b]	Skaftafell	Skaftafellsfjöll	64.08807	-16.97369	hyaloclastite	Upper Gauss	*b*						
isl033		Skaftafell	Skaftafellsfjöll	64.08343	-16.98093	dike margin								
isl034	JM6[b]	Skaftafell	Skaftafellsfjöll	64.08201	-16.98469	pillow margin	Upper Gauss	*b*						
isl035	JM7B[b]	Skaftafell	Skaftafellsfjöll	64.08288	-16.98726	pillow fragments	Upper Gauss	*b*						
isl036		Skaftafell	Skaftafellsfjöll	64.08248	-16.98587	pillow margin								
isl037	HM0 (?)[b]	Skaftafell	Hafrafell	64.00855	-16.87314	flow bottom	$>$ 3.94 $\pm$ 0.06 Ma	*b*						
isl038	HM1 (?)[b]	Skaftafell	Hafrafell	64.00810	-16.87360	pahoehoe flow top	3.94 $\pm$ 0.06 Ma	*b*						
isl039	HM1 (?)[b]	Skaftafell	Hafrafell	64.00810	-16.87360	thin flow	3.94 $\pm$ 0.06 Ma	*b*						
isl040	HM3[b]	Skaftafell	Hafrafell	64.02699	-16.88276	hyaloclastite	3.20 $-$ 3.94 Ma	*b*						
isl041	HM7[b]	Skaftafell	Hafrafell	64.02683	-16.88011	flow top	3.2 $-$ 3.35 Ma	*b*	3	46.93	3.61	7.7	6.56E+22	5.05E+21
isl042	HM15[b]	Skaftafell	Hafrafell	64.02672	-16.87772	flow margin	1.69 $-$ 2.35 Ma	*b*						
isl043	HM31[b]	Skaftafell	Hafrafell	64.02198	-16.86354	poor pillow margin	1.69 $\pm$ 0.29 Ma	*b*						
isl044	HM31[b]	Skaftafell	Hafrafell	64.02224	-16.86370	pillow fragments	1.69 $\pm$ 0.29 Ma	*b*						
isl045	HM11[b]	Skaftafell	Hafrafell	64.02675	-16.87363	flow margin	2.35 $-$ 2.59 Ma	*b*	4	47.06	4.38	9.3	6.58E+22	6.12E+21
isl046	HM8[b]	Skaftafell	Hafrafell	64.02644	-16.87453	sill margin	3.20 $\pm$ 0.09 Ma	*b*						
isl047		Sida	Kálfafell	63.93560	-17.70288	flow top	4 ka	*i*	6	66.48	4.87	7.32	9.30E+22	6.81E+21
isl048	Laki[c], RH10[d]	Sida	Eldvatnstangi	63.89852	-17.73606	pahoehoe flow top	1783 CE	*j*	13	45.12	2.5	5.54	6.31E+22	3.50E+21
isl049		Sida	Landbrotshólar	63.76461	-17.95491	glassy agglutinate	934 CE	*j*						
isl050	BS3[f]	Sida	Merkurheidi	63.79651	-18.06877	hyaloclastite	2.58 Ma	*k*						
isl051	BS2[f]	Sida	Seljalandsheidi	63.91316	-17.81171	pillow margin	2.58 Ma	*k*	6	20.56	1.2	5.83	2.88E+22	1.68E+21
isl052	isl048[a]	Sida	Seljalandsheidi	63.91256	-17.81103	glassy flow top	1783 CE	*j*	Results combined with isl048					
isl053	BS5[f]	Sida	Seljalandsheidi	63.91739	-17.78941	altered pollow breccia	2.58 Ma	*k*						
isl054	BS9[f]	Sida	Seljalandsheidi	63.91735	-17.79268	pillow breccia	2.58 Ma	*k*	6	32.82	1.29	3.94	4.59E+22	1.80E+21
isl055	BS5[f]	Sida	Seljalandsheidi	63.91885	-17.78666	pillow fragment	2.58 Ma	*k*						
isl056	BS5[f]	Sida	Seljalandsheidi	63.91736	-17.78472	hyaloclastite	2.58 Ma	*k*						
isl057		Sida	Seljalandsheidi	63.91763	-17.78318	dike margin	2.58 Ma	*k*	5	23.39	0.63	2.69	3.27E+22	8.81E+20
isl058	BS5[f]	Sida	Seljalandsheidi	63.91775	-17.78188	pillow margin	2.58 Ma	*k*	3	24.57	0.05	0.19	3.44E+22	6.99E+19
isl059		Nupakot	Nupakot Farm	63.54620	-19.66770	dike margin	$\sim$0.78 Ma	*l*						
isl060		Nupakot	Nupakot Farm	63.54607	-19.66775	lava flow bottom	$\sim$0.78 Ma	*l*						
isl061		Nupakot	Sigurger Farm	63.54724	-19.68457	dike margin	$\sim$0.78 Ma	*l*						
isl062		Nupakot	Sigurger Farm	63.54698	-19.68522	hyaloclastite	$\sim$0.78 Ma	*l*						
isl063	BS1[f]	Sida	Merkurheidi	63.79868	-18.05797	hyaloclastite	2.58 Ma	*k*	3	50.58	1.32	2.61	7.08E+22	1.85E+21
isl064	Leit.[c], RH01[d]	WRZ	Raudólar	64.09447	-21.75119	agglutinate	5.254 $\pm$.206 ka	*m*						
isl065		WRZ	Raudólar	64.09514	-21.75180	flow top	7 $-$ 11 ka	*g*	7	59.66	2.04	3.42	8.33E+22	2.85E+21

Continued on next page

Table 1 – continued from previous page

Site	Alt. Name	Region	Location	Lat (°N)	Lon (°E)	Sample Type	Age	Age Ref.	nn	B_F	$B_{F\sigma}$	$B_{F\sigma}$ %	VADM	VADM$_\sigma$
isl066	Kap.[c]	WRZ	Háibruni	64.00761	-21.92108	flow bottom	0.799 ka	*n*						
isl067		WRZ	Bugda	64.09901	-21.78453	pillow margin	Early Brunhes	*g*						
A2		WRZ	Thórólfsfell	64.44878	-20.51725	pillow margin	Weichsel	*a*						
A3		WRZ	Hödufell	64.42900	-20.57036	pillow margin	Late Weichsel	*o*						
A4		WRZ	Fagradalsfjöll-1	64.45283	-20.30611	pillow margin	Late Weichsel	*o*						
A6		WRZ	Bláfjall	64.51564	-19.88783	pillow margin	Saale	*a*						
A8		WRZ	Thverbrekknamúli-2	64.72322	-19.61464	pillow margin	Weichsel	*a*	5	78.45	2.22	2.83	1.09E+23	3.09E+21
A11		ERZ	Hnottóttaalda	64.52200	-18.47167	pillow margin	Weichsel	*a*						
A15	ICE08R-11[a,e]	ERZ	Vatnsfellsvirkjun	64.20183	-19.05564	pillow margin	Weichsel	*a*	7	19.03	0.73	3.83	2.66E+22	1.02E+21
A24		ERZ	Mid-Bálkafell	64.67300	-17.76611	pillow margin	Weichsel	*a*	4	62.19	5.03	8.09	8.66E+22	7.00E+21
A26		ERZ	Vonarskard	64.69231	-17.89653	pillow margin	Weichsel	*a*	3	40.1	2.83	7.05	5.58E+22	3.94E+21
A27		ERZ	Kirkjufellsvatn	63.97903	-18.89628	pillow margin								
A28		ERZ	Klappagil	63.97414	-18.79219	pillow margin	Weichsel	*a*	4	31.19	1.87	5.98	4.36E+22	2.61E+21
A29		ERZ	Hördufell	63.96903	-18.67975	pillow margin	Weichsel	*a*						
A30		ERZ	Hellnaá	64.06139	-18.53400	pillow margin	Weichsel	*a*	3	29.09	0.65	2.25	4.06E+22	9.08E+20
A31		ERZ	Hrútabjörg	64.11031	-18.46158	pillow margin	Weichsel	*a*	3	59.5	0.59	0.99	8.31E+22	8.24E+20
A32		ERZ	NW of Grænifjallgardur	64.10578	-18.51542	pillow margin								
A33		ERZ	Breidbak	64.10594	-18.56867	pillow margin								
A34		ERZ	Hnausar	64.08778	-19.05417	pillow margin	Weichsel	*a*	8	30.67	1.11	3.61	4.28E+22	1.55E+21
A35	islhhj[a,e]	ERZ	Sigalda	64.17217	-19.13853	pillow margin	Weichsel	*a*	5	12.84	0.85	6.59	1.79E+22	1.19E+21
A38	ICE08R-25[a,e]	ERZ	Fellsendavatn	64.18847	-18.95700	pillow margin								
HEL-2		WRZ	Helgafell	64.01606	-21.84244	pillow margin	Early Weichsel	*g*	4	44.91	3.84	8.54	6.28E+22	5.37E+21
HRA-1		WRZ	Hraunsvik	63.85192	-22.36867	pillow margin	Late Weichsel	*g*						
HS92-15	islhhc,k[a,e]	NRZ	Bláfjall	65.42664	-16.81561	pillow margin	$\sim$14 ka	*o*	9	31.39	0.87	2.77	4.35E+22	1.21E+21
HS92-16	islhhl[a,e]	NRZ	Bláfjall	65.42511	-16.81606	pillow margin	$\sim$14 ka	*o*	8	33.04	1.41	4.26	4.58E+22	1.95E+21
ICE08R-07		WRZ	Stakur	63.99644	-21.88872	pillow margin	Early Weichsel	*g*						
ICE08R-08	A12[a,e]	ERZ	N- and S-Hágöngur	64.56969	-18.19967	pillow margin								
ICE08R-09	A13[a,e]	ERZ	Skerdhingar-1	64.57161	-18.07064	pillow margin								
ICE08R-10	A16[a,e]	ERZ	Bláfjall	64.37169	-18.24844	pillow margin	Weichsel	*a*						
ICE08R-12	A18[a,e]	ERZ	Outcrop close to Dór	64.38131	-18.25056	pillow margin								
ICE08R-13		ERZ	Bláfjall	64.38956	-18.22922	pillow margin								
ICE08R-14	A19[a,e]	ERZ	Ljósufjöll	64.24325	-18.58269	pillow margin	Weichsel	*a*	6	28.58	0.21	0.72	3.99E+22	2.93E+20
ICE08R-15	A20[a,e]	ERZ	Kambsfell	64.82736	-17.75550	pillow margin	Weichsel	*a*	3	33.06	1.9	5.75	4.60E+22	2.64E+21
ICE08R-16	A21[a,e]	ERZ	Gnjótsá	64.82686	-17.70228	pillow margin	Weichsel	*a*						
ICE08R-18	A23[a,e]	ERZ	Gully near Valafell	64.72367	-17.72217	pillow margin								
ICE08R-19	A25[a,e]	ERZ	Svarthöfdhi	64.64253	-17.86858	pillow margin	Weichsel	*a*						
ICE08R-20		ERZ	Fontur, craters	64.25175	-18.65233	pillow margin	Weichsel	*a*						
ICE08R-23	A36[a,e]	ERZ	Heljargjá	64.32217	-18.46050	pillow margin	Weichsel	*a*	3	36.1	3.77	10.44	5.04E+22	5.26E+21
ICE08R-24	A37[a,e]	ERZ	Miklagljúfur	64.32050	-18.43261	pillow margin	Weichsel	*a*	3	35.24	3.22	9.13	4.92E+22	4.49E+21
KVIH-1		NRZ	Kvihólafjöll	65.84017	-16.98622	pillow margin	Weichsel	*a*						
KVK117		NRZ	Lindafjöll	64.86700	-16.35000	pillow margin	Weichsel	*a*	7	25.94	1	3.87	3.61E+22	1.39E+21
KVK118		NRZ	Kverkfjöll	64.76700	-16.63300	pillow margin								
KVK119		NRZ	Kverkfjöll	64.76700	-16.50000	pillow margin								
KVK77		NRZ	Kverkfjöll	64.81667	-16.48333	pillow margin	Weichsel	*a*	6	20.29	3.18	15.69	2.82E+22	4.42E+21
LON-1		WRZ	Lönguhlíðar	63.97172	-21.94506	pillow margin	Early Weichsel	*g*						
MAE-1		WRZ	Mælifell	64.10706	-21.18192	pillow margin	Late Weichsel	*g*						
NAL-213	islhhh[a,e]	NRZ	Hvammsfjöll	65.36383	-16.67408	pillow margin								
NAL-352		NRZ	Upptyppingar			pillow margin	48 ± 7 ka	*p*						
NAL-356	islhhd[a,e]	NRZ	Upptyppingar	65.03300	-16.23300	pillow margin	Weichsel	*a*	7	34.8	1.9	5.45	4.83E+22	2.64E+21
NAL-440	islhhe[a,e]	NRZ	Hrímalda	64.92483	-17.08558	pillow margin	Early Weichsel	*a*						
NAL-455	islhhf[a,e]	NRZ	Kverkfjöll	64.73842	-16.62225	pillow margin	$<$0.78 Ma	*q*	4	43.69	1.98	4.53	6.08E+22	2.76E+21
NAL-460		NRZ	Theistareykir/Kistufjall	65.87917	-17.15561	pillow margin	Early Brunhes	*g*	3	25.41	1.59	6.27	3.51E+22	2.20E+21
NAL-500		NRZ	Gæsavatn	64.78061	-17.51131	pillow margin	Weichsel	*a*	4	30.79	1.41	4.59	4.28E+22	1.96E+21
NAL-584	islhhb[a,e]	NRZ	Dyngjufjöll Ytri	65.16169	-16.92431	pillow margin	Weichsel	*a*	6	35.3	3.55	10.07	4.90E+22	4.93E+21
NAL-585		NRZ	Upptyppingar	65.02797	-16.22900	pillow margin	Weichsel	*a*						
NAL-595	islhhg[a,e]	NRZ	Kistufell	64.78994	-17.18231	pillow margin	Weichsel	*a*	7	62.38	5.33	8.55	8.68E+22	7.41E+21
NAL-611	islhha,i[a,e]	NRZ	Kistufell	64.79844	-17.20033	pillow margin	Weichsel	*a*	14	57.62	4.59	7.97	8.02E+22	6.39E+21
NAL-828		NRZ	Hrúthálsar	64.32381	-16.50278	pillow margin								
NAL-837		NRZ	Kvihólafjöll	65.84017	-16.98622	pillow margin	Weichsel	*a*						
RET-1/VES-1		SIVZ	Réttarfell (Thórsmörk)	63.67208	-19.49233	pillow margin								
REY-1		WRZ	Reykjanes viti	63.81239	-22.71367	pillow margin	$0 - 1.2$ ka	*g*						
THREN-1		WRZ	Threngsli	64.00133	-21.46261	pillow margin	Early Weichsel	*g*						
VIF-1		WRZ	Vífilsfell	64.04872	-21.54022	pillow margin	Early Weichsel	*g*						

Table 2. Selection statistics at the specimen and sites levels and their threshold values. See text for a brief definition of each criterion.

Specimen						
SCAT	*FRAC*	*Gap Max*	β	*MAD*	*DANG*	$\lvert\vec{k}'\rvert$
-	≥ 0.78	≥ 0.60	≤ 0.10	$\leq 5.0^\circ$	$\leq 10.0^\circ$	≤ 0.164
Site						
nn	B_σ	B_σ %				
≥ 3	≤ 4 μT	≤ 10 %				

Table 3. Median paleointensity results for grouped sites. Groups are based on stratigraphic age controls with approximate age ranges listed in kyrs. The number of sites per group is N. B_F and VADM are the median intensity and virtual axial dipole moment, B_{Fmad} and VADM$_{mad}$ are their respective median absolute deviations.

Group	Age Range (ka)	N	B_F (μT)	B_{Fmad} (μT)	VADM (ZAm^2)	VADM$_{mad}$ (ZAm^2)
Holocene	0-11	4	55.8	15.6	78.1	22.0
Late Weischel	11-20	5	33.0	8.1	45.8	11.7
Early Weischel	20-110	4	37.7	4.9	52.7	7.0
Weischel	11-110	20	33.9	5.8	47.2	8.0
Brunhes	11-780	4	28.4	2.8	39.7	4.1
Matuyama/Gauss	$\sim$2580	6	28.7	6.7	40.2	9.4
Gauss	3200-3500	1	46.9	3.6	46.9	5.1
All sites	0-3500	44	34.9	9.8	48.6	13.9
All Weischel	11-110	29	34.8	6.4	48.3	9.2
All Brunhes (ex-Hol)	11-780	33	33.1	7.2	46.0	10.2
All (ex-Holocene)	11-3500	40	33.1	8.3	47.0	11.6

Table 4. Mean paleointensity results (μT) for the 1783 C.E. Laki lava flow, sampled in this study and by *Stanton et al.* [2011] and *Tanaka et al.* [2012].

	Laki Flow (1783 C.E.)
This Study	45.12 $\pm$ 2.5, nn=13
Stanton et al. [2011]	47.6 $\pm$ 5.1, nn=6
Tanaka et al. [2012]	51.5 $\pm$ 1.7, nn=4